FATIGUE MODELING OF COMPOSITE OCEAN CURRENT TURBINE BLADE

by

Mohammad Wasim Akram

A Thesis Submitted to the Faculty of

The College of Engineering and Computer Science

in Partial Fulfillment of the Requirements for the Degree of

Master of Science

Florida Atlantic University
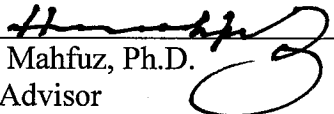
Boca Raton, Florida

December 2010

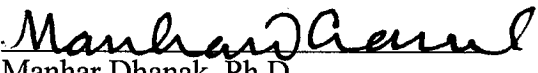# FATIGUE MODELING OF COMPOSITE OCEAN CURRENT TURBINE BLADE

by

Mohammad Wasim Akram

This thesis was prepared under the direction of the candidate's thesis advisor, Dr. Hassan Mahfuz, Department of Ocean and Mechanical Engineering, and has been approved by the members of his supervisory committee. It was submitted to the faculty of the College of Engineering and Computer Science and accepted in partial fulfillment of the requirements for the degree of Master of Science.
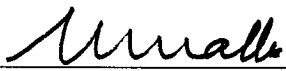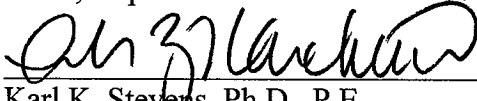
SUPERVISORY COMMITTEE:
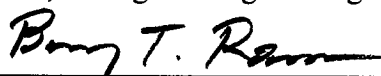
Hassan Mahfuz, Ph.D.
Thesis Advisor

Manhar Dhanak, Ph.D.

Francisco Presuel-Moreno, Ph.D.

Frederick Driscoll, Ph.D.

Mohammad Ilyas, Ph.D.
Chair, Department of Ocean and Mechanical Engineering

Karl K. Stevens, Ph.D., P.E
Dean, College of Engineering and Computer Science

Barry T. Rosson, Ph.D.
Dean, Graduate College

November 15, 2010
Date

ACKNOWLEDGEMENTS

ABSTRACT

Author :   Mohammad Wasim Akram

Title: Fatigue Modeling of Composite Ocean Current Turbine Blade

Institution: Florida Atlantic University

Thesis Advisor: Dr Hassan Mahfuz

Degree: Master of Science

Year: 2010

The success of harnessing energy from ocean current will require a reliable structural design of turbine blade that is used for energy extraction. In this study we are particularly focusing on the fatigue life of a 3m length ocean current turbine blade. The blade consists of sandwich construction having polymeric foam as core, and carbon/epoxy as face sheet. Repetitive loads (Fatigue) on the blade have been formulated from the randomness of the ocean current associated with turbulence and also from velocity shear. These varying forces will cause a cyclic variation of bending and shear stresses subjecting to the blade to fatigue. Rainflow Counting algorithm has been used to count the number of cycles within a specific mean and amplitude that will act on the blade from random loading data. Finite Element code ANSYS has been used to develop an S-N diagram with a frequency of 1 Hz and loading ratio 0.1 Number of specific load cycles from Rainflow Counting in conjunction with S-N diagram from ANSYS has been utilized to calculate fatigue damage up to 30 years by Palmgren-Miner's linear hypothesis.

TABLE OF CONTENTS

LIST OF FIGURES

LIST OF TABLES

xiii

1.   INTRODUCTION

1.1   General

In this era of Green Clean Energy, the energy from Ocean Current can be a vital source of sustainable energy. South Florida, one of the most densely populated areas in the United States, is largely confined to a strip of land between the Atlantic Ocean and the Everglades. The urbanized area (that is, the area of contiguous urban development) is about 110 miles (180 km) long (north to south), but never more than 20 miles (32 km) wide, and in some areas only 5 miles (8.0 km) wide (east to west)[1]. Atlantic Ocean can be the cleanest and the most abundant source of renewable energy for South Florida. The Gulf Stream [2-3] Current flows northward past the southern and eastern shores of Florida, funneling through the Florida Straits with a mass transport greater than 30 times the total freshwater river flows of the world (i.e. over eight billion gallons per minute [4]. The extraction of energy from ocean current is in developing stages compare to other conventional and renewable energy technologies. In addition, commercial ocean energy harvesting systems do not exist today. Although many single technology-centric efforts are underway around the world, there is no unifying infrastructure in the United States or abroad to support wider, multi-resource and multi-technology development. Florida Atlantic University's Center for Ocean Energy Technology is making bridge between

1

those gaps [4]. But before that a small-scale experimental ocean current turbine is required to install for investigating and collecting data about potential environmental impacts as well as to design a reliable structure for the blades. A pilot project is being considered with a rotor blade of 6m diameter part of underwater turbine design to produce 129KW.

In order to succeed in this project, a structural design is needed to ensure that the blade, one of the major components of the Ocean Current Turbine (OCT) system, can withstand all likely loading during service. The random nature of ocean current means the blade will experience a significant number of fatigue cycles over its expected lifespan of 25-30 years. As a consequence, a suitable fatigue analysis must be undertaken in the structural design stage to ensure that the blade has adequate life. This thesis focuses on the development of composite ocean current turbine blades by performing static and fatigue load analyses, and predicting of fatigue life from the random load spectrum.

1.2   Ocean Current Turbines: Installation and Blade Materials

1.2.1   Currently Installed Ocean Current Turbines

The concept of energy extraction from ocean current is relatively new. Seaflow, the world's first offshore tidal turbine of 300 kW, was installed only 7 years ago in 2003 by Marine Current Turbine Ltd. at 3km North East of Lynmouth on the North Devon coast of England [5]. The mono-pile support structure was designed for 20m to 40m depth locations and the turbine unit was designed for a current between 2m/s and 3 m/s [5]. Figure 1.1 shows the photograph of Seaflow during its maintenance period.

Figure 1.1: Seaflow during the first installation

(Courtesy: Marine Current Turbine Ltd.)

After the success of Seaflow, MCT Limited developed a more energy and cost efficient mono-pile design utilizing twin 16m diameter rotor blades. The project is called 'SeaGen,' [6] and was just recently installed in Strangford Lough, Northern Ireland in April 2008. Each mono-pile SeaGen (Figure 1.2) unit is capable of producing 1.2 MW, which makes it the world's first megawatt-scale tidal turbine installed.

Figure 1.2: Seagen, world's first Megawatt marine current turbine

(Courtesy: Marine Current Turbine Blade Ltd.)

In 2006 Verdant Power installed their first grid-connected free flow turbine (Figure 1.3) in New York City's east river, along the eastern shore of Roosevelt Island [7]. Later, in May 2007 they connected the proposed remaining turbines to form an array of six, making Verdant Power the world's first company to connect an array of turbines to a grid.

Figure 1.3: Verdant Power's marine current turbine

(Courtesy: Verdant Power)

Verdant Power's project in the East River uses turbines with 5m rotor diameters that rotate at 32 rpm and are capable of producing 35KW each [7]. Their design operates fully beneath the surface and does not affect boat traffic. Verdant's system is ideal for shallow water areas, where large arrays can be installed to produce power, but as with the SeaGen unit, it cannot be installed in deepwater. To date, there has been no successful installation of a horizontal axis ocean current turbine in water in excess of 40m deep. Florida Atlantic University (FAU) plans to pass this mark, proposing to harness energy from the Gulf Stream Current with an array of underwater ocean current turbines.

4

1.2.2 Materials of Ocean Current Turbine Blade

The 11 m diameter Seaflow rotor blades are made up of steel and fiberglass, which is shown in figure 1.4. A longitudinal steel spar gives the blade the bulk of its spanwise strength and stiffness. The steel chordwise ribs provide lateral strength and help transfer torsion to the steel spar. The fiberglass skin also provides strength and stiffness, and helps load distribution.

Figure 1.4: Cross-section of Seaflow turbine blade (Steel and Fiber Glass)

Performances of steel structure underwater are poor due to low corrosion resistance and heavy weight. Any rotating component always contributes to fatigue loads due to continuous change of point of gravity. So this is very important to neutralize the body forces. Lighter materials with high stiffness to weight ratio can attain this criterion by balancing body forces with buoyancy loads. On the other hand, hollow section can fail the component by buckling.

There are some researches on ocean current turbine blade but most of them are based on hydrodynamic design or energy conversion methods. There is no significant research on

5

material of ocean current turbine blades. W.M.J. Batten et al. [8-10] have studied much more on prediction of the hydrodynamics performance of ocean current turbine. N. Asseff and H. Mahfuz [11] have studied the material for ocean current turbine blades under static loads. They have found that using filler materials instead of hollow section can resist the failure against buckling. They also designed the model for neutral weight. They have used sandwich composite for blade materials. This sandwich structure has several advantages for using in marine environment including high corrosion resistance, high stiffness to weight ratio and high fatigue resistance. However, they did not study the fatigue performance of their modeled blade. Besides these, there is no research found so far for ocean current blade. Though some works are available on offshore structure and materials but those will not be applicable for deep Ocean. Hence fatigue analysis of the blade is required for a safe and reliable structural design.

1.3   Past Works on Fatigue of Sandwich Composites

Sandwich composites are extensively used these days in structural applications such as components in spacecrafts, aircrafts, marine vessels, transportation structures and so on where minimum structural weight and maximum stiffness/strength is important. It has also good resistance in marine environment due to high resistivity against corrosion. These features have made sandwich structure as number one choice for ocean current turbine blades. In such applications, composite sandwich structures are often subjected to the repeated loading which may lead to fatigue failure. The life time events in sandwich composite materials and structures under long term cyclic loading conditions form a complex process. Several damage mechanisms may grow and interact to alter the state of

6

material, change the stress distribution, and define the life of the structure. This complex phenomenon has attracted a lot of researchers to work in this field [12]. Hence extensive works are available on fatigue of sandwich structures. Each work has its own geometry, load ratio, frequency and damage model.

Analytical models for many aspects of mechanical behavior of sandwich composites have been discussed elaborately by Vinson [13] and Zenkert [14]. Vast majority of the fatigue related works are available on fiber-reinforced composite, not sandwich structures. From limited amount of work done on analytical modeling of fatigue of composite sandwich structures that has been reported in the literature seem to be based on a lifetime prediction using S-N curves. Kanny and Mahfuz [15-16] derived a simple expression based on S-N approaches for predicting the fatigue life of foam core sandwich beams.

Bruman and Zenkert [17-18] also proposed a simple curve fitting S-N approaches using two Weibull function and found reasonable agreement between experimental and analytical results. Sendeckyj [19] briefly reviewed another fatigue damage model by considering deterioration of the initial strength during fatigue life. Based on similar lines, Dain and Hahn [20] developed a wear out model, based on the concept of strength degradation to assess the fatigue behaviors of sandwich beams. El Mahi et al. [21] developed a model based on the stiffness reduction approach for sandwich composites. But this approach has limited application. The applicability of such approaches to sandwich structures seems to be limited to face sheet tension or compression fatigue, where as core shear seems to be dominant mode of fatigue failure in foam core sandwich structures.

The most widely used approach is the Palmgren-Miner criterion or linear damage rule. To utilize this approach for sandwich composites Hashin and Rotem [22], Wang et al. [23] modified the Miner's model and have found very good accuracy. Clark et al. [24] have done research on cumulative damage modeling of sandwich beams based on the stiffness degradation approach. Most of the above mentioned researches required experimental data for the modeling. These data from experiment may vary due to experimental conditions and environments. Three point bending and four point bending data are very common. Shenoi and Wellicome [25] have published a book on composite materials in marine structure.

Till to date not a single work is available on fatigue analysis of OCT blade. And also unlike what has been studied in the literature, service loads on OCT blade will be random in nature which will make the fatigue phenomena more complex.

1.4 Motivations

(1)   In this century, the challenge for the world is to reduce usage of fossil fuel. So, every research institute is now focusing on Green clean energy. This will be a golden opportunity for FAU's Center of Ocean Energy and Technology to lead in renewable energy generation, moving away from carbon based fuel systems, by extracting electrical energy from strong gulfstream current. The success of this ocean energy conversion system depends on a reliable and safe operational design which includes the material selections, structural stability analysis based on failure criterion and stress-strain analysis. For continuous power supply the structure needs to be withstanding at least 20-30 years under static and fatigue loads. In this long life cycle, the structure will be subjected to

repeated load or impact load which may cause failure to the components and damage the entire system catastrophically. In this thesis, a reliable design for the turbine blades has been investigated under static and fatigue loading for safe operation.

(2)   The concept of harnessing energy from ocean current is comparatively new with respect to other renewable energy sources. Design of any structural component in marine environment is challenging due to randomness of ocean waves, movement of sea-animal, corrosion and so on. Moreover there is no research so far reported on this. Most of the researches are based on hydrodynamic prediction, while one or two may be on structural aspect. But so far, no research has been conducted on the fatigue of the marine current turbine blades although this is an important issue from structural point of view.

(3)   Sandwich composites have been chosen as blade's material. There are extensive works on fatigue of the sandwich composite. But fatigue modeling is mostly empirical and it behaves differently in different loading condition, geometries, loading frequency and loading sequences. As OCT will be installed at below 50m depth from water surface, so it's fatigue modeling will not be identical with previous researches. That's why it is novel to study the fatigue modeling of sandwich composite in this specific application.

1.5   Problem Statement

The OCT blade is expected to withstand under all likely loads during its operation for at least 25 years. The OCT blade will be subjected to both static and fatigue loads. The blade will be under high static loads due to high density of sea water. On the other hand, fatigue loads will be originated from randomness of ocean current associated with turbulence, velocity shear, and so on. The blade will also be in corrosive marine

environment. Therefore, selection of materials and modeling of an OCT blade under both static and fatigue loads are required. It is necessary to ensure a safe operational life cycle of the OCT blade for successful energy harvesting.

1.6   Structure of the Thesis

In chapter 2, the fatigue terminology is defined along with the approaches of the fatigue analysis. Non constant amplitude loading history is also discussed. Rainflow Counting Algorithm and Linear Fatigue Model are explained. These are important for predicting life cycles. Failure theories associated with sandwich materials are also included.

In the following chapter, materials for OCT blade and sources of fatigue loads are discussed. Sandwich structure is suggested for turbine materials. Therefore, definition of sandwich structure and advantages of using that in marine environment is included. Loading spectrum originated from different sources is extracted using Rainflow Counting Algorithm.

Chapter 4 reports the finite element simulation technique. This chapter includes selection of materials and element types, application of static and fatigue loads. Meshing method and algorithm of fatigue analysis are also included.

In chapter 5, results from Rainflow Counting and Finite Element Simulation are included and discussed. Life time prediction using Palmgren-Miner's method is also been calculated. This chapter shows the results graphically and using contour plots. The influences of various components on the life prediction are also discussed.

Summary and recommendations for future works are made in the final chapter. Blade Element theory and loads from velocity of ocean current are included in Appendix. At the end of the thesis bibliography is attached.

2.   THEORETICAL BACKGROUNDS

2.1   Fatigue

Any load that varies with time can potentially cause fatigue failure [26-27]. The character of theses loads may vary substantially from one application to another. In rotating machine, the loads tend to be consistent in amplitude over time and repeat with the same frequency. In service equipment (in our case), the loads tend to be quite variable in amplitude and frequency over time and may even be random in nature. Usually the shape of the waveform of the load-time function does not to have any significant effect on fatigue failure. Therefore we usually depict the function schematically as a sinusoidal form. The stress-time waveform has the same general shape and frequency as the load-time waveform. The significant factors are the amplitude and the average value of the stress-time waveform and the total number of stress cycle that the part will experience. Some basic definitions about fatigue phenomena and variation of service equipment loading are discussed in the following sections.

2.2   Approaches of Fatigue

2.2.1   Total-Life Approaches

Classical approaches to fatigue design involve the characterization of total fatigue life to failure in terms of the cyclic stress range (the S-N curve approach) or the strain

range. In these methods, the number of cycles necessary to induce fatigue failure estimated under controlled amplitude cyclic stresses or strains. The resulting fatigue life incorporates the number of fatigue cycles to initiate a dominant crack and to propagate this dominant flaw until the catastrophic failure occurs. Various techniques are available to account for the effect of mean stresses, stress concentrations, environments, multi-axial stresses and variable amplitude stress fluctuations in the prediction of total fatigue life using classical approaches. Since the crack initiation life constitutes a major component of the total fatigue life (which can be as high as 85% to 90% of the total fatigue life) [26], these approaches represent, in many cases, design against crack initiation. Researches on sandwich composite by this approach also reveal that for sandwich structure crack initiation life if 85% of total fatigue life.

2.2.2 Defect-tolerant approach

The fracture mechanics approach [28] to fatigue design, on the other hand, invokes a 'defect-tolerant' philosophy. The basic premise here is that all engineering components are inherently flawed. The size of pre-existing flaw is generally determined from non destructive testing. The useful fatigue life is then defined as the number of fatigue cycles or time to propagate the dominant crack from initial size to some critical dimension. The choice of the critical size for the fatigue crack may be based on the fracture toughness of the material, the limit load for the particular structural part, the allowable strain or the permissible change in the compliance of the component. The prediction of crack propagation life using the defect-tolerant approach involves empirical crack growth laws based on fracture mechanics. This method is applicable under

13

conditions of small-scale yielding, where the crack tip plastic zone is small compared to the characteristics dimensions of the cracked component and where predominantly elastic loading conditions prevail. This intrinsically conservative approach to fatigue has been widely used in fatigue-critical applications where catastrophic failures will result in the loss of human lives; examples include nuclear industries and boiler industries.

2.2.3   Safe-Life Approach

The safe-life approach was developed by aerospace engineers [26]. It is also used for wind turbine design. In safe-life approach to fatigue design, the typical cyclic load spectra, which are imposed on a structural component in service, are first determined. On the basis of this information, the components are analyzed or tested in laboratory under load conditions which are typical of service spectra, and a useful fatigue life is estimated for the component [29]. At the end of the expected safe operation life, the component is automatically retired from service, even if no failure has occurred during service. The safe life approach is intrinsically   theoretical in nature. This procedure invariably has to account for several unknowns, such as unexpected changes in load conditions, variation in properties among different batches of same material, existence of initial defects in the production process, corrosion of the parts used in the component, and human errors in the operation of the component. By selecting a large margin of safety, a safe operating life can be guaranteed, although such a conservative approach may not be desirable from economical point of view. The ocean current turbine will be installed at 50m depth from sea surface. It will not be easily accessible from time to time. On the other hand, for an initial design it is expensive for testing the entire blade against fatigue loading. Therefore,

14

this approach is useful for modeling ocean current turbine blade under fatigue loading with a design of 25-30 years safe-life (which is extensively used for wind turbine industries).

2.3   Basic Fatigue Parameters

Generally the stress time functions experienced can be modeled as shown in figure 2.1, which shows them schematically as sinusoidal wave form. Figure-2.1(a) shows the fully reversed case for which the mean value is zero. Figure (b) shows a repeated stress case in which the waveform ranges from zero to a maximum with a mean value equal to the alternating component, and Figure 2.1(c) shows one version of the more general case (called fluctuating stress) with all components values non zero. Any of this waveform can be characterized by two parameters, their mean and alternating components, their maximum and minimum values, or ratios of these values.
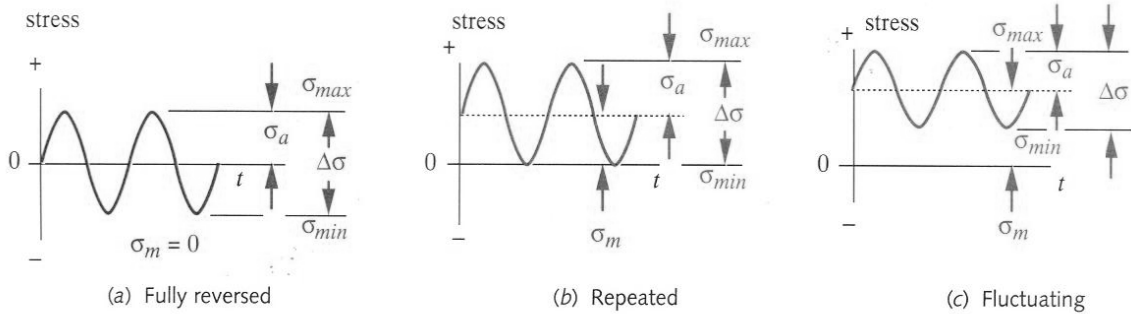
Figure 2.1: Fully reversed, repeated and fluctuating cyclic stresses

The stress range, $\Delta\sigma$ is defined as

$$\Delta\sigma = \sigma_{max} - \sigma_{min} \tag{1}$$

The alternating component σ_a is found from

15

$$\sigma_a = \frac{\sigma_{max} - \sigma_{min}}{2} \qquad (2)$$

The mean component, σ_m is

$$\sigma_m = \frac{\sigma_{max} + \sigma_{min}}{2} \qquad (3)$$

Stress Ratio, $R = \frac{\sigma_{min}}{\sigma_{max}}$ \qquad (4)

Stress Level, $S = \sigma_m + \sigma_a$ \qquad (5)

All of these parameters are important for fatigue modeling. Any change of these parameters has a significant effect on the fatigue life. However these parameters are obtained from ideal case. For service equipment loadings these parameters will not be so uniform.

2.4 Service Equipment Loading

The loading spectrum for service equipment is not so easily defined as for rotating machine as discussed above. Some examples of these in service stress-time waveforms are shown in figure 2.2, which depicts a general loading case in (a), a typical pattern for wind turbine in (b), and a pattern typical of a common aircraft in (c). These patterns are semi-random in nature as the events do not repeat with any particular period. Data such as these are generally used in computer simulation programs that calculate the cumulative fatigue damage.
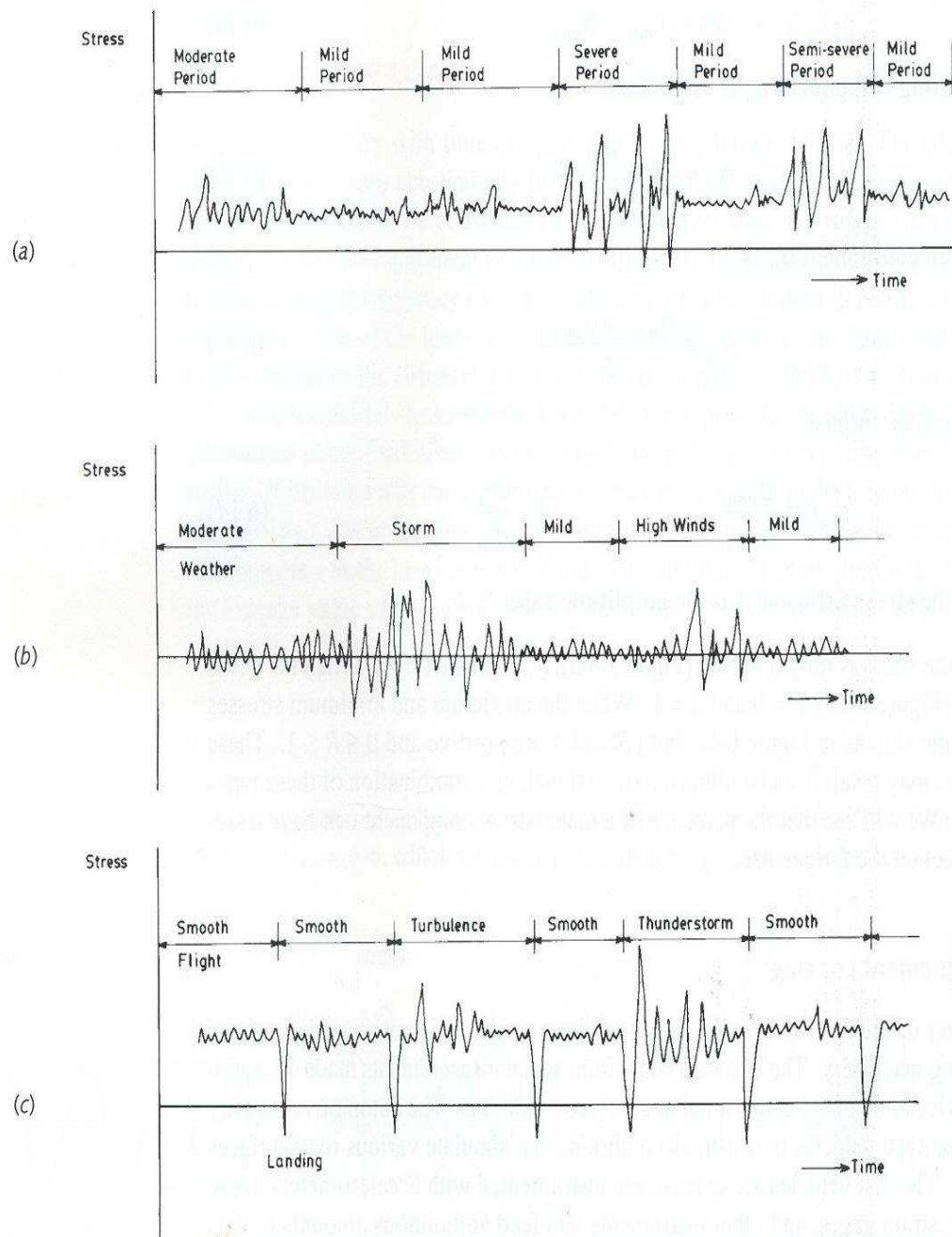
Figure 2.2: Semi random loading [30]

2.5   Fatigue Design Process

To be effective in averting failure, the designer should have a good working knowledge of analytical and empirical techniques of predicting failure so that during the pre-described design, failure may be prevented. That is why; the failure analysis, prediction, and prevention are of critical importance to the designer to achieve a success. Fatigue design is one of the observed modes of mechanical failure in practice. For this reason, fatigue becomes an obvious design consideration for many structures, such as ocean current turbine, wind turbine, aircraft, bridges, railroad cars, automotive suspensions and vehicle frames. For these structures, cyclic loads are identified that could cause fatigue failure if the design is not adequate. The basic elements of the fatigue design process are illustrated in Figure 2.3.
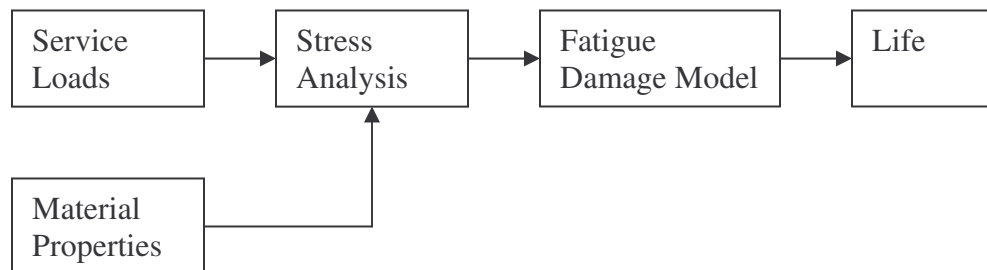
Figure 2.3: The basic elements of the fatigue design process

2.6   Service and Operational Loads on Turbine Blades

Ocean current turbine blades are designed with a load carrying main spar that supports an outer hydrodynamic shell. Globally the blade should be sufficiently stiff in order to resist collide between the tower and blades during operational and extreme

loading. Locally the spar together with the stiffness of the outer shell ensures that the shape of the hydrodynamic profile is maintained as stable as possible. There are some similarities in loading on wind turbine [31-32] blade and ocean current turbine blade. The major loads on ocean current turbine blades are -

1. Flapwise and edgewise bending due to hydrodynamic loads on the blade.

2. Gravitational loads, which changes the magnitude due to change of center of gravity due to rotation of turbine blade. This load will contribute in edgewise bending loading.

3. Buoyancy Loads.

4. Torsion loading because the shear resultant of flapwise and edgewise loads do not go through the shear center of the blade section.

5. Centrifugal loads due to rotation of the blade. It contributes to flapwise bending loading and depends on the rpm of the turbine.

6. Relative small loads due to acceleration and deceleration.
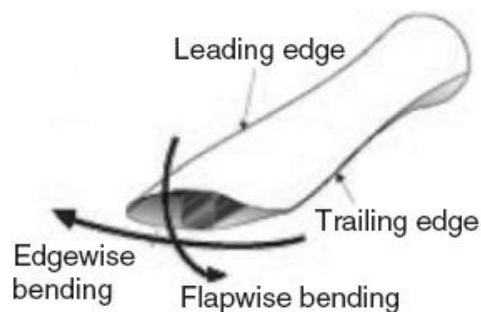
Figure 2.4: Flapwise and Edgewise Bending (Both Ocean Turbine and Wind Turbine)

The later three have negligible influence on the design loads, and it is the flapwise and edgewise loads that determine the structural design and the blade cross section.

The design has been emphasized on neutral buoyant conditions for efficient power production by equalizing the weight of the blade. On the other hand, the weight will create fluctuating sinusoidal loads due to rotation of the blades if it would not be neutralized. Fatigue loading will not create either gravity or buoyancy loads. As discussed earlier, there are some fundamental differences in operating OCT and wind turbines. One of them is contribution of centrifugal forces to the flapwise bending.

2.7   Cumulative Damage Analysis

Life prediction or damage analysis for a component or structure consists of several closely interrelated steps as can be seen in figure 2.1. A combination of the load history (Service Loads), stress concentration factors (Stress Analysis) and cyclic stress-strain properties of the materials are important for damage analysis. One of the most simple and convenient cumulative fatigue damage models is the Palmgren-Miner's linear method. This method is suitable for random loading histories and for computer simulation.

2.7.1 Palmgren-Miner Rule

This fatigue model originally suggested by Palmgren (1924) and later developed by Miner (1945). This linear theory is referred to as the Palmgren-Miner rule or the linear damage rule.

The theory has some assumptions based on loading histories which is well applicable for random loading cycles in the field of fatigue analysis in ocean current turbine, wind turbine and aero plane. The assumptions are given below-

I)   Linearity: It assumes that all cycles of a given magnitude do the same amount of damage, whether they occur early or late in the life.

ii)   Non-interactive: It assumes that the presence any stress cycle does not affect the damage caused by other stress cycles.

iii)   Stress independent: It assumes that the rule governing the damage caused by a stress cycles is the same as that governing the damage caused by another stress cycles.

Almost all available fatigue data for design purposes is based on constant amplitude tests. However, in practice, the alternating stress amplitude may be expected to vary or change in some way during the service life when the fatigue failure is considered. The variations and changes in load amplitude often referred to as spectrum loading, make direct use of S-N curves inapplicable because these curves are developed and presented for constant stress amplitude operation. The key issue is how to use the mountains of available constant amplitude data to predict fatigue in a component. In this case, to have an available theory or hypothesis becomes important which is verified by experimental observations. It also permits design estimates to be made for operation under conditions of variable load amplitude using the standard constant amplitude S-N curves that are more readily available. Many different cumulative damage theories have been proposed for the purposes of assessing fatigue damage caused by operation at any given stress level and the addition of damage increments to properly predict failure under conditions of

21

spectrum loading. Collins, in 1981, provided a comprehensive review of the models that have been proposed to predict fatigue life in components subject to variable amplitude stress using constant amplitude data to define fatigue strength.

Life estimates may be made by employing Palmgren-Miner rule along with a cycle counting procedure. Target is to estimate how many of the blocks can be applied before failure occurs. This theory may be described using the S-N plot.

In this rule, the assumptions can be summarized as follows:

i)   The stress process can be described by stress cycles and that a spectrum of amplitudes of stress cycles can be defined. Such a spectrum will lose any information on the applied sequence of stress cycles that may be important in some cases.

ii)   A constant amplitude S-N curve is available, and this curve is compatible with the definition of stress; that is, at this point there is no explicit consideration of the possibility of mean stress.
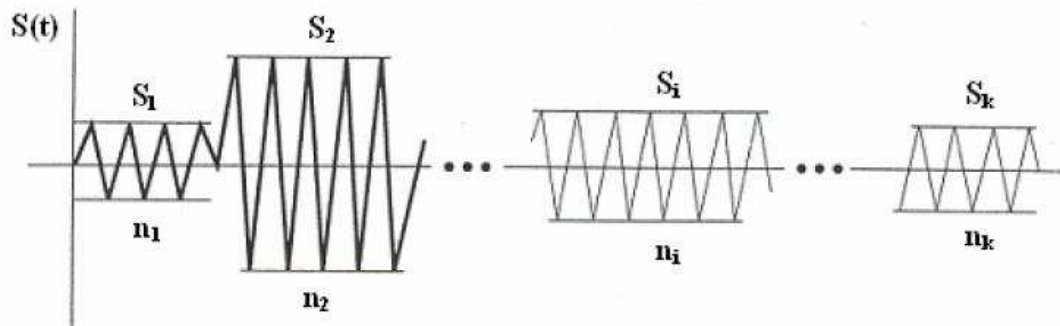
Figure 2.5: Spectrum of amplitudes of stress cycles

22

In Figure 2.5, a spectrum of amplitudes of stress cycles is described as a sequence of constant amplitude blocks, each block having stress amplitude S_i and the total number of applied cycles n_i. The constant amplitude S-N curve is also shown in Figure 2.6.
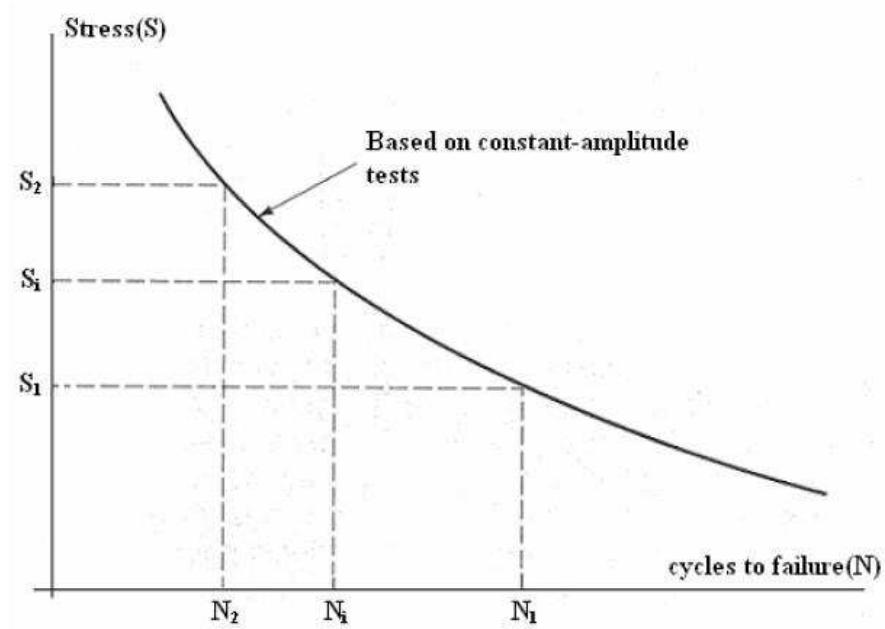
Figure 2.6: Constant amplitude S-N curve

By using the S-N data, number of cycles of S_1 is found as N_1 which would cause failure if no other stresses were present. Operation at stress amplitude S_1 for a number of cycles 'n_1' smaller than N_1 produces a smaller fraction of damage which can be termed as D_1 and called as the damage fraction.

Operation over a spectrum of different stress levels results in a damage fraction D_i for each of the different stress levels S_i in the spectrum. It is clear that, failure occurs if the fraction exceeds unity-

$$D_1 + D_2 + D_3 + - - - - - + D_{i-1} + D_i \geq 1.0 \qquad (6)$$

According to the Palmgren-Miner rule, the damage fraction at any stress level S_i is linearly proportional to the ratio of number of cycles of operation to the total number of cycles that produces failure at that stress level that is-

$$D_i = \frac{n_i}{N_i} \tag{7}$$

Then, a total damage can be defined as the sum of all the fractional damages over a total of k blocks,

$$D = \sum_{i=1}^{k} D_i = \sum_{i=1}^{k} \frac{n_i}{N_i} \tag{8}$$

And the event of failure can be defined as $D \ge 1.0$

2.8   Rainflow Counting Method

Most of the fatigue damage model has been developed based on constant amplitude loading. But in operation loadings are not such ideal as mentioned in the beginning of the article. In most cases, loadings are random in nature. One of the cases of random stress history is shown in figure 2.7.
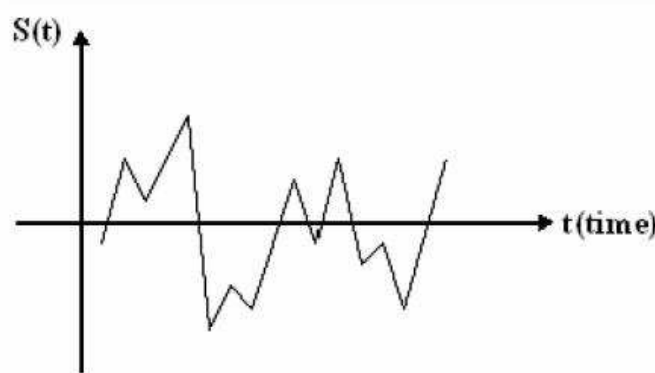
Figure 2.7: Random Loading Histories

Extraction of load histories from these types of random loading is difficult. In general, a random stress S(t) is not only made up of a peak alone between two passages by zero, but also several peaks appear, which makes it difficult to determine the number of cycles absorbed by the structure. The counting of peaks makes it possible to constitute a histogram of the peaks of the random stress which can then be transformed into a stress spectrum giving the number of events for lower than a given stress value. The stress spectrum is thus a representation of the statistical distribution of the characteristic amplitudes of the random stress as a function of time.

This Rainflow counting algorithm is very important for fatigue analysis specifically where loads are random in nature. The loads on ocean current turbine blades due to hydrodynamic are dependent of ocean current. Therefore loads will also be random like ocean current. As a result, a statistical load history is required for simulation. Loading histories based on Rainflow Counting[33] has been considered in this investigation as input for simulation work. The load will be weighted by their amplitude and number of occurrences.

For any fatigue analysis, the starting point is the response of the structure or component, which is usually expressed as a stress or strain time history. If the response time history is made up of constant amplitude stress or strain cycles then the fatigue design can be accomplished by referring to a typical to a typical S-N diagram. However, because real signals rarely confirm to this ideal constant amplitude situation, an empirical approach is used for calculating the damage caused by stress signals of variable amplitude. Despite its limitations, Palmgren- Miner rule is used for this purpose. This linear relationship assumes that the damage caused by parts of a stress signal with a particular range can be

calculated and accumulated to the total damage separately from that caused by other ranges. When the response time history is irregular with time as shown in Figure 2.8, Rainflow cycle counting is used to decompose the irregular time history into equivalent stress of block loading.
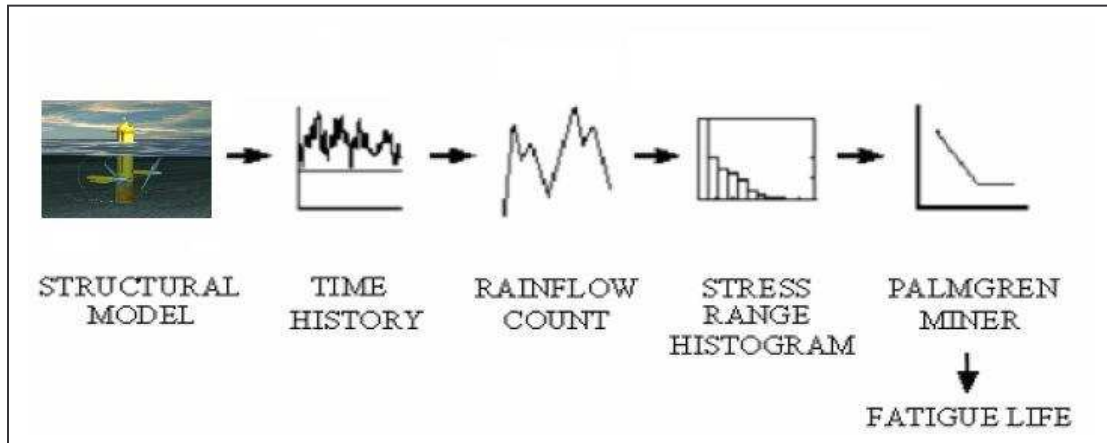
Figure 2.8: Steps involved in fatigue calculation by rainflow counting and ANSYS

The number of cycles in each block is usually recorded in a stress range histogram. Finite Element code is used to develop an S-N diagram. Number of cycles from Rainflow Counting in conjunction with S-N diagram from ANSYS is used to calculate damage using Palmgren-Miner's method.

2.9   Failure Theories

Failure means a component has separated into two or more pieces, has become permanently distorted, and has had its reliability downgraded. In case sandwich composite failure can occur when delamination starts between skin and core. As sandwich composite consists of core and skin material so two types of failure will be associated with ultimate failure of the component. Tsai Wu failure criteria will be

appropriate for defining failure of the composite. On the other hand, distortion energy theory can be a good approximation for defining failure theory of the core as core is considered as isotropic material. In this thesis, these two failure criteria have been used.

2.9.1 Distortion Energy Theory and Von-Mise's Theory

The unit volume subjected to any three dimensional stress state designated be σ_1, σ_2, and σ_3 is shown in figure 2.9 [27]. The stress state can be divided into two portions: one is hydrostatic tension due to stresses σ_{av} acting on each of the same principle directions and the other one is distortional component. Due to hydrostatic component the element undergoes pure volume change, that is, no angular distortion. If we regard σ_{av} as a component of σ_1, σ_2, and σ_3, then this component can be subjected from triaxial stress state to get the distortion component. This distortion element is subjected to pure angular distortion i.e. no volume change.
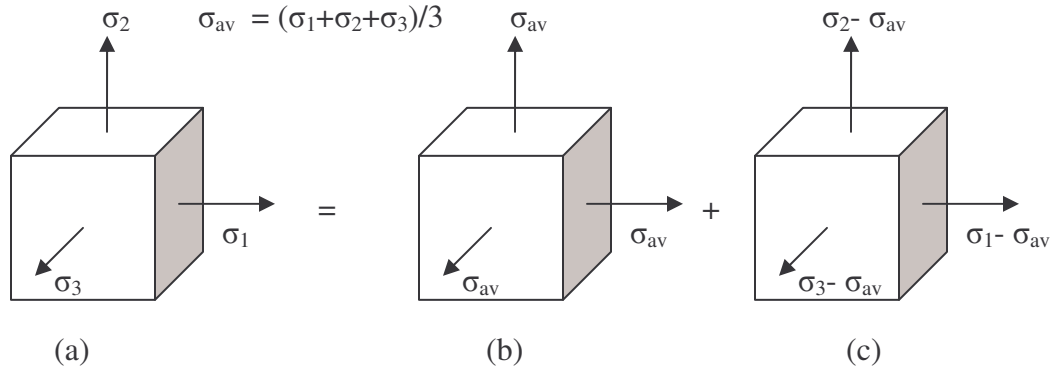
Figure 2.9: Element with (a) triaxial, (b) hydrostatic, (c) distortional component

27

The strain energy per unit volume for simple is - $U = \frac{1}{2}\varepsilon\sigma$. Where 'ε' and 'σ' are strain and stress respectively. For the element of figure X-X (a) the strain energy per unit volume is $U = \frac{1}{2}\left[\varepsilon_1\sigma_1 + \varepsilon_2\sigma_2 + \varepsilon_3\sigma_3\right]$ (9)

For a stress element undergoing σ_x, $\sigma_{z,\ and}$ σ_z simultaneously, the normal strains are given by generalized Hook's law [32]

$$\varepsilon_x = \frac{1}{E}\left[\sigma_x - v\left(\sigma_y + \sigma_z\right)\right]$$

$$\varepsilon_y = \frac{1}{E}\left[\sigma_y - v\left(\sigma_x + \sigma_z\right)\right] \qquad (10)$$

$$\varepsilon_z = \frac{1}{E}\left[\sigma_z - v\left(\sigma_x + \sigma_y\right)\right]$$

The constant properties 'E' and 'υ' are Young's Modulus and Poisson's ratio respectively. Substituting equation (10) in equation (9) –

$$U = \frac{1}{2E}\left[\sigma_1^2 + \sigma_2^2 + \sigma_3^2 - 2v\left(\sigma_1\sigma_2 + \sigma_2\sigma_3 + \sigma_3\sigma_1\right)\right] \qquad (11)$$

Now strain energy for volume change only can be written in term of σ_{avg} –

$$U_v = \frac{3\sigma_{av}^2}{2E}\left(1 - 2v\right) \qquad (12)$$

The distortion energy is obtained by subtracting equation (12) from equation (11)-

$$U_d = \frac{1+v}{3E}\left[\frac{(\sigma_1 - \sigma_2)^2 + (\sigma_2 - \sigma_3)^2(\sigma_3 - \sigma_1)^2}{2}\right] \qquad (13)$$

For the general state of stress given by yield is predicted if –

$$\left[\frac{(\sigma_1 - \sigma_2)^2 + (\sigma_2 - \sigma_3)^2 + (\sigma_3 - \sigma_1)^2}{2}\right]^{\frac{1}{2}} \geq S_y \qquad (14)$$

The left of equation (14) is termed as equivalent or effective stress for the entire general state of stress given by σ_1, σ_2, and σ_3. This effective stress is called von Mises stress, σ^V, named after Dr. R.Von Mises who contributed to the theory.

2.9.2 Tsai Wu Failure Criteria

The Tsai-Wu criterion is a simplified version of a general failure theory for orthotropic materials which was earlier developed by Gol'denblat and Kopnov. By assuming the existence of a failure surface in the stress plane, a modified tensor polynomial theory was proposed by Tsai and Wu [34-35] . Further assumptions, including transverse isotropy about the 2-3 planes, made it possible to arrive at the following expression for the failure index:

$$I_F = \frac{1}{\left[-\dfrac{B}{2A} + \sqrt{\left(\dfrac{B}{2A}\right)^2 - \dfrac{1}{A}}\right]} \qquad (15)$$

Where

$$A = \frac{\sigma_1^2}{F_{1t}F_{1c}} + \frac{\sigma_2^2}{F_{2t}F_{2c}} + \frac{\sigma_3^2}{F_{3t}F_{3c}} + \frac{\sigma_4^2}{F_4} + \frac{\sigma_5^2}{F_5} + \frac{\sigma_6^2}{F_6} + c_4\frac{\sigma_2\sigma_3}{\sqrt{F_{2t}F_{2c}F_{3t}F_{3c}}} + c_5\frac{\sigma_1\sigma_3}{\sqrt{F_{1t}F_{1c}F_{3t}F_{3c}}} +$$

$$c_6\frac{\sigma_1\sigma_2}{\sqrt{F_{1t}F_{1c}F_{2t}F_{2c}}} \qquad (16)$$

$$B = \left(\frac{1}{F_{1t}} - \frac{1}{F_{1c}}\right)\sigma_1 + \left(\frac{1}{F_{2t}} - \frac{1}{F_{2c}}\right)\sigma_2 + \left(\frac{1}{F_{3t}} - \frac{1}{F_{3c}}\right)\sigma_3 \qquad (17)$$

Here, σ_i = Principal stress in the i th direction , i = 1,2,3

29

σ_{jk} = Shear Stress; j,k = 1,2,3

F_{ij} = Strength in the i th direction with j denoting tension or compression

c_i = Shear Coupling Coefficient in the i th direction

3.   MATERIALS AND LOADING

3.1   Sandwich Structure

Structural sandwich is a special form of laminated composite comprising of a combination of different materials that are bonded to each other so as to utilize the properties of each separate component to the structural advantage of the whole assembly. Structural members those are made of two stiff, strong skins separated by a lightweight core are known as sandwich panels (ASTM definition). The separation of the skins by a low density core increases the moment of inertia of the beam/panel with little increase in weight producing an efficient structure. The faces are adhesively bonded to the core to obtain a load transfer between the components. The construction of a sandwich structure and the stresses developed in different components of sandwich structure under flexural loading are shown in figure 3.1.
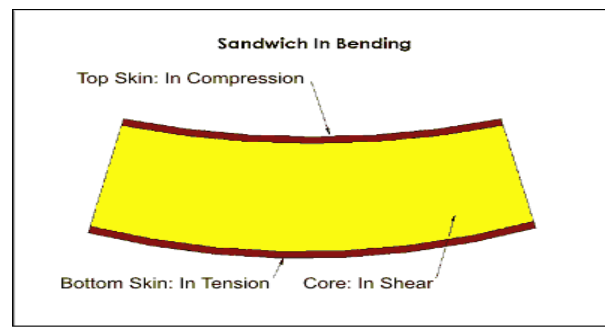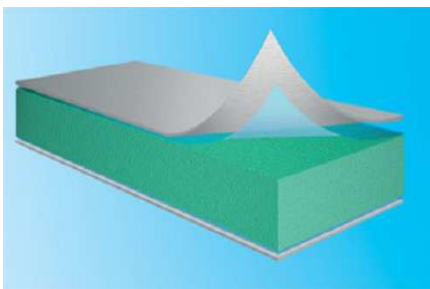
Figure 3.1: A sandwich composite (left) and loaded sandwich structure (right)

3.2   Advantages of Sandwich Structure

The use of a sandwich construction in a composite design is well suited for a structure requiring high in-plane and flexural stiffness. A sandwich panel is comprised of two thin face sheets, or skins, and a lightweight, thicker, low-stiffness core. The skin takes almost all the bending and in-plane loads, while the core helps stabilize the skin against buckling. The core defines the flexural stiffness, out-of-plane shear and compressive behavior. For example, when using a sandwich construction with foam core and two identical face sheets, the flexural stiffness increases with the square of the core height [11].

(a) Sandwich Construction   (b) Monocoque Construction
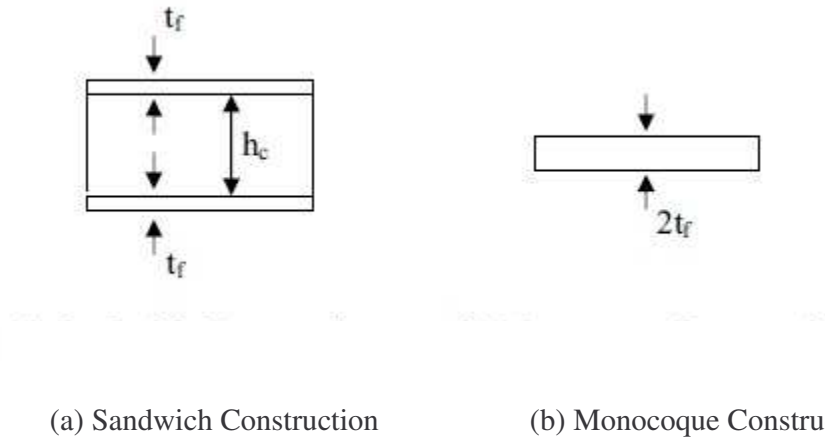
Figure 3.2: Sandwich and monocoque construction

$$\frac{D_s}{D_m} = \frac{3}{4}\left[\frac{h_c}{t_f}\right]^2 \tag{19}$$

Here, D_s = Flexural stiffness of sandwich structure, D_m = Flexural Stiffness of monocoque construction. h_c and t_f are thickness of the core and face respectively.

As a result, if $\dfrac{t_f}{h_c} = \dfrac{1}{20}$ the flexural stiffness of the sandwich construction would be three hundred times that of the monocoque construction. In addition, the ratio of the bending stress (σ_s) in a sandwich face to the maximum stress (σ_m) in a monocoque structure of approximately the same weight is [11]-

$$\frac{\sigma_s}{\sigma_m} = \frac{2t_f}{3h_c} \qquad\qquad (20)$$

Therefore if $\dfrac{t_f}{h_c} = \dfrac{1}{20}$ the bending stress in the sandwich will be 1/30th of the monocoque of approximately the same weight. In conjunction with sandwich construction, webs can be added to further strengthen and stiffen a laminate.

A web will help support the skin by absorbing more than a negligible part of the load. The flexural stiffness of a web core sandwich is dependent on the depth and thickness of the web. The stiffness increases due to the increase in the area moment of inertia by the added vertical composite laminate(s). Web will also increase the out-of-plane shear strength. Using of sandwich composite has several other advantages besides those above mentioned structural advantages. It has high energy absorption capability, buoyancy and high resistance against corrosion.

The ocean current turbine blade will be operated in marine environment at 50m depth from sea surface. At such depth, the corrosion due to salinity of the sea water will have severe effect on the blade materials. On the other hand, the density of the sea water is comparatively high (1025 kg/m^3). Therefore, hydrodynamic force will be also higher. To withstand these extreme conditions materials such as a sandwich construction will be

33

advantageous. Turbine blade may experience impact loads due to movement of sea animal or strong surface hurricane. Sandwich construction can easily absorb energy due to these transient loading cases. The sandwich component for a OCT blade is shown in figure 3.3.
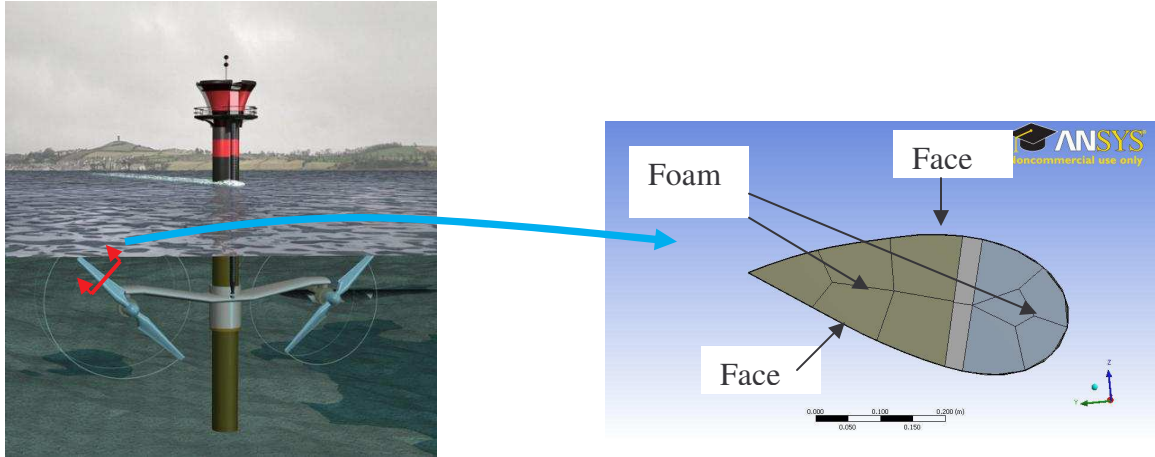
Figure 3.3: Ocean current turbine blade material

Advantages of sandwich construction for OCT are shown in below:

Table 3.1: Advantages of sandwich structures for Ocean Current Turbine Blade

Properties of sandwich construction	Underwater application
High Corrosion Resistivity	In seawater at 50m depth salinity is about 35 psu (practical salinity unit) which may cause corrosion damage.
High Stiffness and Strength	Hydrodynamic forces are related with the density of the sea water which is 1025 kg/m^3. Due to this high density

	hydrodynamic force will be higher.
High Energy Absorption	Transient load due to movement of sea animal and strong hurricane can cause impact loading.
High Fatigue Resistance	Due to randomness of the ocean current and turbulence effect, the loading on ocean current turbine blade will vary.
Buoyancy and weight	Buoyancy force and gravitational forces are needed to be neutralized.

3.3   Materials of Blade Component

3.3.1   Hydrodynamic Shell

Material for hydrodynamic shell should have high modulus and strength as this will be subjected on high hydrodynamic loads due to high density of sea water. Beside this, it should have high corrosion resistance and also hydrodynamic formability. Adherence to internal structure as well as neutral weight in water is also important properties that should be possessed by hydrodynamic shell materials. Carbon/Epoxy has almost all of these properties. It has a modulus of 143 GPa and tensile strength of 2240 MPa which is very high in comparison with other composite materials. Density of carbon/epoxy is 1620kg/m^3 which is much lower than steel. Composite materials are also less corrosive in marine water. From the properties mentioned above for hydrodynamic shell material, Carbon/Epoxy seems be a good selection.

3.3.2 Material for Web

Web materials should have high adhesiveness with adjoin components, high shear modulus, and neutral weight in water. Carbon/Epoxy and S2-Glass/Epoxy both have almost same properties. But the web materials should have the anchoring capability to connect blade with the hub. S2-Glass/Epoxy has good capability for this purpose than carbon/epoxy [11]. It is also cheaper than carbon/epoxy. As the web will not carry any load so the material cost should be low. Hence from economical as well as structural point of view, S2-Glass/Epoxy has been selected as web material.

3.3.3 Core Material

The core materials should have high buckling resistance, water impermeability and neutral weight in water. As it will be connected with skin and web so it should also have high adhesiveness. Divinycell [36] cores provide an ideal balance between performance and cost. In addition to their strength to weight ratios, they have excellent ductile qualities to make them ideal for a wide range of applications where impact or slamming loads are likely to be experienced. Other features include excellent dimensional stability, low water absorption and chemical resistance.

Divinycell is available in a variety of grades and densities to match a broad range of application performance requirements. Divinycell HCP grade has been selected for the core materials of the blade as its buoyancy grade which offers excellent hydraulic compressive properties. It has been developed to meet the demand for a light weight, high performance buoyancy material. This grade is used not only in ocean current turbine blade but also light weight sea vessel, yacht and offshore structure. The density of core is

100 kg/m^3. At that density, each blade will have approximately 7 kg of buoyancy. The design was made buoyant to compensate for the speculated metal/composite joint. Designing the blades to be neutrally buoyant will make power production more efficient by canceling the body force resisting the blades rotation.

3.4   Sources of Fatigue Loads

Loading spectrum is one of the most important parameters for fatigue analysis. A loading spectrum may contain mean and amplitude of loading, sequences of loading, frequencies and number of repetition of any specific loading cycle. Laboratory tests are done mostly with constant amplitude and frequency for fatigue analysis. However, service loads will not be always constant in amplitude and frequency. So, a definite loading spectrum is required for fatigue analysis of any component in operation. Before determining loading spectrum of the turbine blade, sources of fatigue loads on turbine blade have been discussed.

OCT blade will be subjected to several fatigue loads in operation. These alternating loads can be originated from a variety of sources. These may includes –

- Randomness of ocean current due to low tide and high tide.
- Velocity shears i.e. variation of ocean current velocity with depth.
- Stochastic loads from turbulence
- Transient load from gusts due to strong hurricane
- Impact loads due to movement of large sea animal
- Periodic loads due to gravity
- Temperature variation with respect to depth

Among all of these sources randomness of ocean current and velocity shear will be dominant. These two loadings will result alternating flapwise bending. Alternative flapwise bending is responsible for more than 90% of the damage in the both wind turbine [37] and ocean turbine blade. Because of this, flapwise bending has been considered for fatigue analysis.

3.5 Randomness of Ocean current and Turbulence

Ocean current is random in nature. It varies due to lunar effect of low tide and high tide, seasonal rainfall and turbulence. The mean velocity of ocean current always varies with respect to time. It can vary hourly or monthly or annually. The variation will be intensified if turbulence is added with this varying mean current. As loads on turbine blade are related with the velocity of ocean current, varying ocean current will always cause a change in loads on turbine. The varying loads on OCT will create alternating bending as well as shear stresses.

To calculate loading variations originating from these sources, about 3 hours or 10000 sec of time history loading or velocity data were considered. But this is a complex task and requires some costly experimental setup. To avoid this experiment, Palmgren-Miner's model has been considered for fatigue analysis as discussed in chapter two. This fatigue model is capable of calculating damage based on an approximation of overall distribution of ocean current velocity. Load sequences have no effect on fatigue life. But stress level and their repetitions are more important which can be found from the counting method.

The Gulf Stream Ocean current follows Normal Distribution [38]. From this distribution a time series of 10000 sec ocean current velocity data have been extracted. From this time series data of ocean current, loading on turbine blade were calculated using Blade Element Theory (BET) as described in Appendix. For a conservative design approach, maximum mean of ocean current as well as maximum standard deviation have been used. With this randomness, 15% of turbulence intensity was added. Time series of velocity data with randomness and turbulence is shown in figure – 3.4.
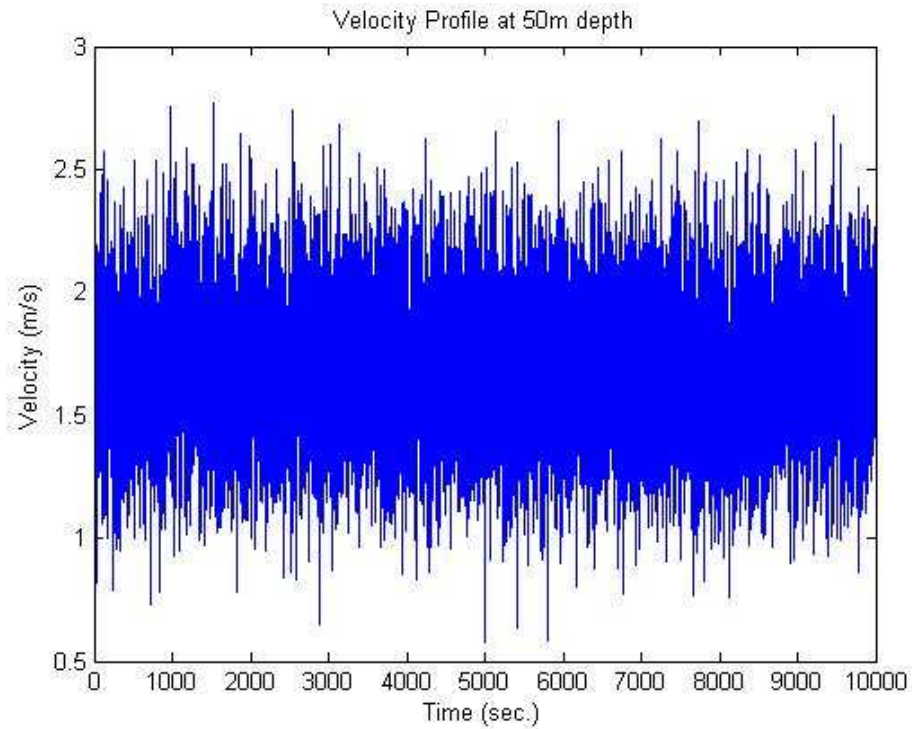
Figure 3.4: Time series of Ocean Current Velocity

From time series velocity data, loads on turbine blade were determined using Blade Element Theory (BET) and MATLAB which has been discussed in the Appendix. These loads followed a normal distribution with a mean of 40KPa and a standard deviation of

12KPa. The loading variation on turbine blade is shown in figure 3.5. It was assumed that the loadings on the blade follow the change of ocean current instantaneously
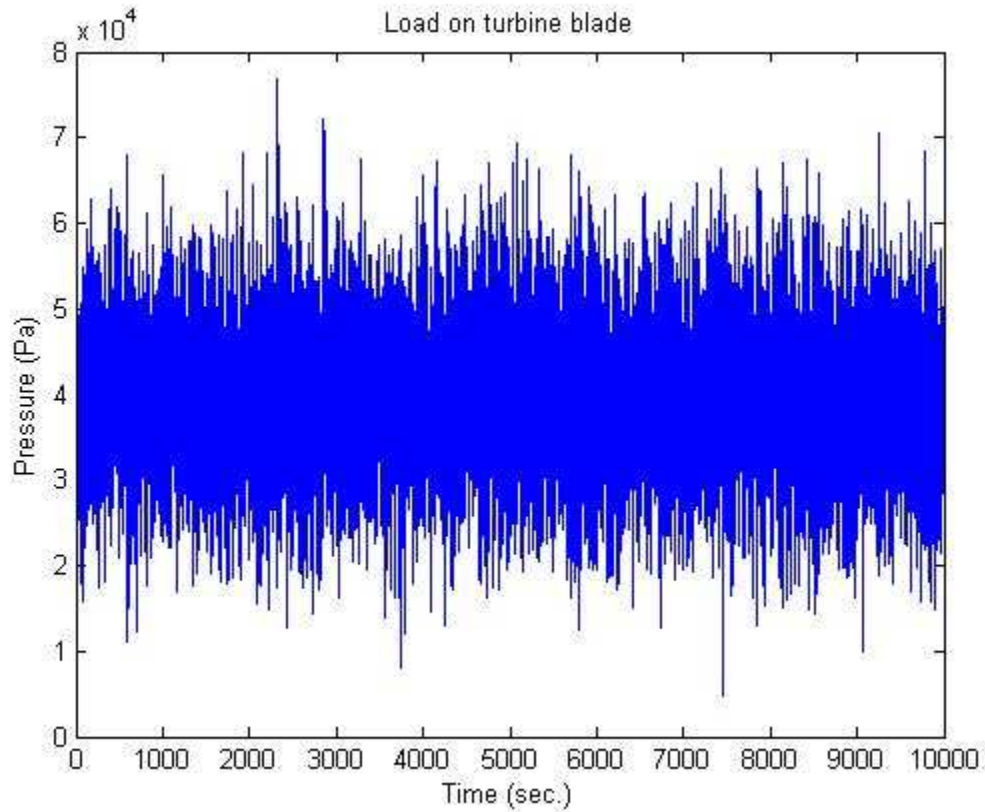
Figure 3.5: Time series of loading on ocean current

From the above figure it is clear that the amplitudes of loading are not constant. To account for these variable amplitude, Rainflow Counting method i.e. cycle counting method was employed to reduce the random load history into a series of discrete events which can be analyzed by ANSYS using constant amplitude fatigue loads. A 3-D view of loading is shown in figure 3.6. From this figure, number of cycles with specific loading amplitude was determined.
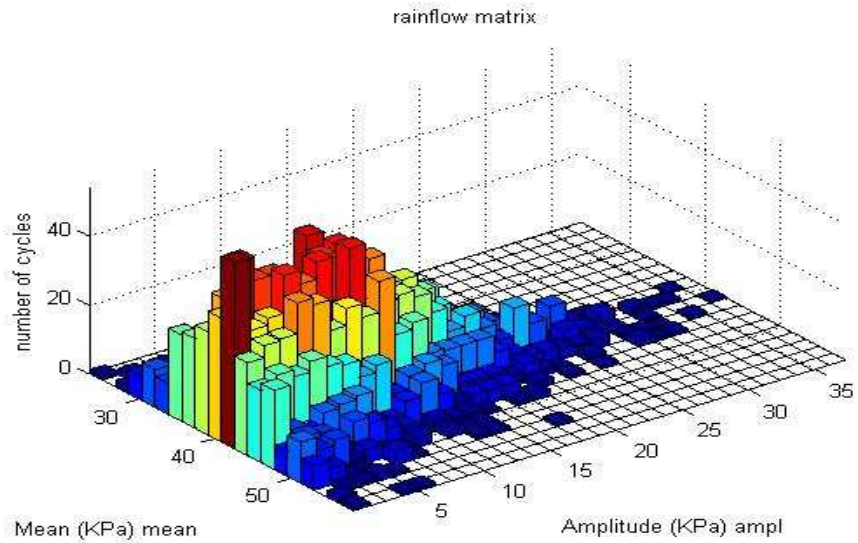
Figure 3.6: Rainflow matrix

From the rainflow matrix it was revealed that most of the loads have low amplitude. But there are some loads with higher amplitude. These loads will cause fatigue failure of the blade. Most of the loads had a mean about 40KPa. Alternating value of the loading also varied. From counting cycle total numbers of cycles with specific alternating amplitude are summarized below in table 3.2.

Table 3.2: Amplitude and number of cycles

Amplitude Range(KPa)	Number of Cycles (in 10,000 sec)
>35	7
30-35	15
25-30	35
20-25	140

15-20	350
10-15	830
5-10	1010
0-5	1160

3.6   Variation of Loads Due To Velocity Shear

The velocity of ocean current varies along with the depth of sea water. Theoretically it follows $1/7^{th}$ power rule [8]. But site specific data is more accurate to predict the velocity distribution with respect to depth. Such velocity distribution at various depths is shown in figure 3.7. It is clear from the figure that as we approach deeper into sea water the velocity will decrease and develop a condition for velocity shear. For example, the change of ocean current velocity is about 0.3 m/s for a change of 20m. So, a large turbine with a diameter of 10 to 20 m will create significant amount of alternating loads on turbine blades as it will be rotating in a varying velocity regime. However for a small scale OCT the variation of alternating loads will not be too high. There will be a 2% load variation at tip for each revolution of the turbine blade. The rotation and the velocity profile are shown in figure 3.8. The load variation for each revolution of the blade is also b shown in figure 3.9. It is noted that this variation will be sinusoidal in nature.

current magnitude (meter/sec), 26° 4.3 N 79° 55 W, 02/26/2009-03/23/2010
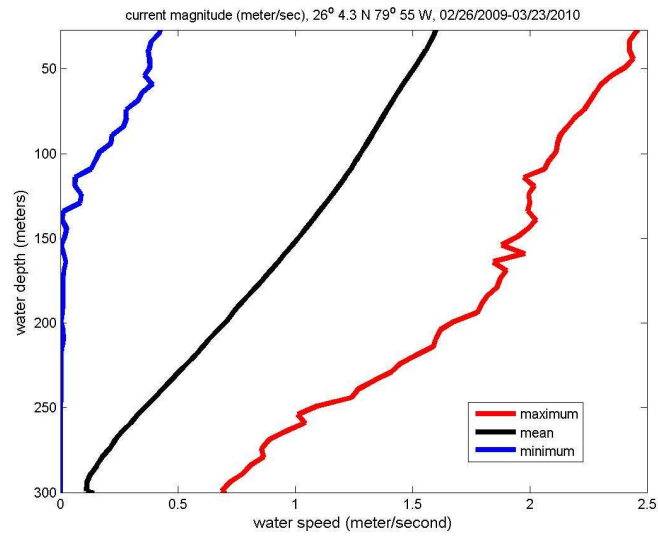
Figure 3.7: Velocity Shear at 50m depth

[Source: ADCP Data Buoy 2 by James VanZweiten, Ph. D.]
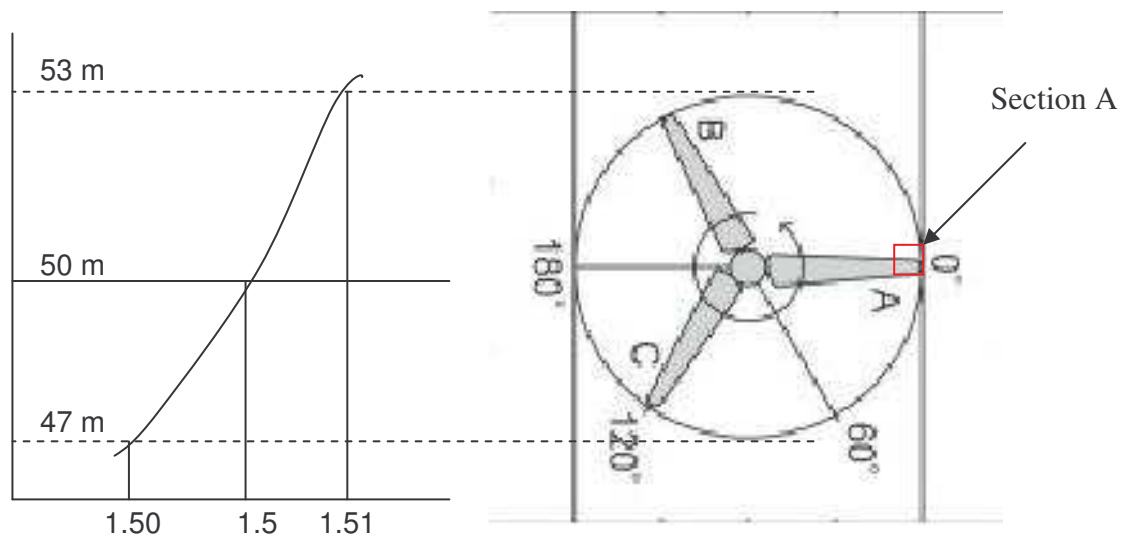
Figure 3.8: Velocity difference for single revolution of turbine blade

43
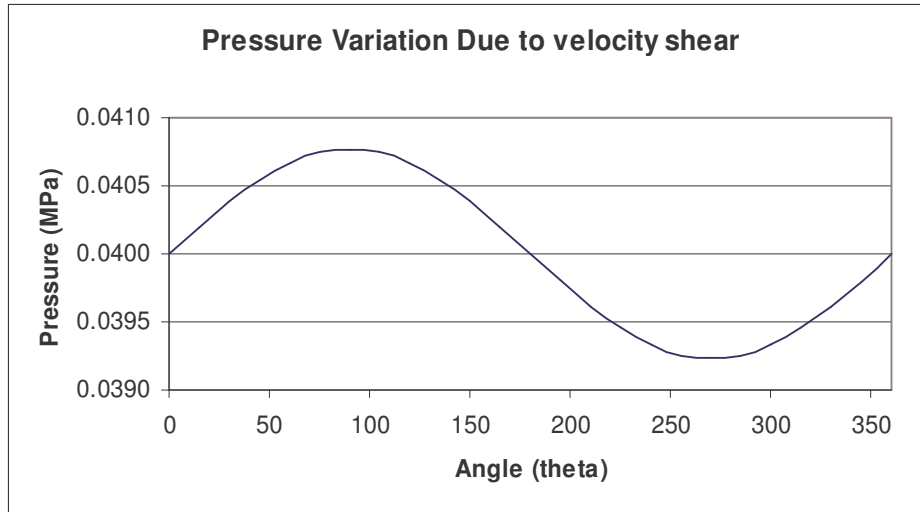
Figure 3.9: Load variation for single revolution of turbine blade

3.7   Loading Spectrum

In this study, two sources of loading variations have been considered. The loading variations due to randomness of ocean current with 15% turbulence have been shown in rainflow matrix and loading variation due to velocity shear has been shown in figure 3.9. The entire loading spectrum was developed based on superposition principle. The frequencies of the all type of loads have been taken as 1 Hz. The superimposed load will have the same mean but different amplitude. For example, two loading spectrums are shown in figure 3.10 and 3.11 respectively.
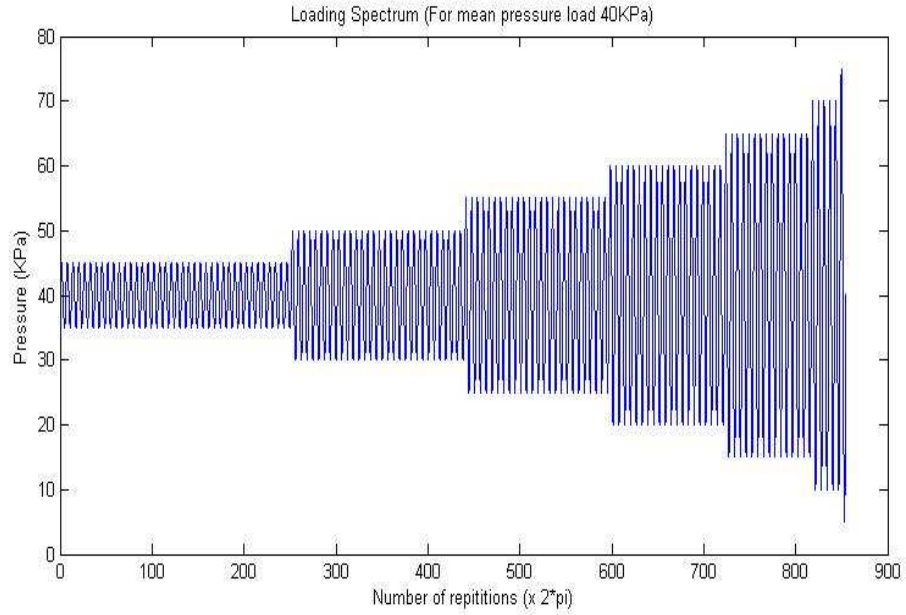
Figure 3.10: Loading spectrum for constant mean pressure
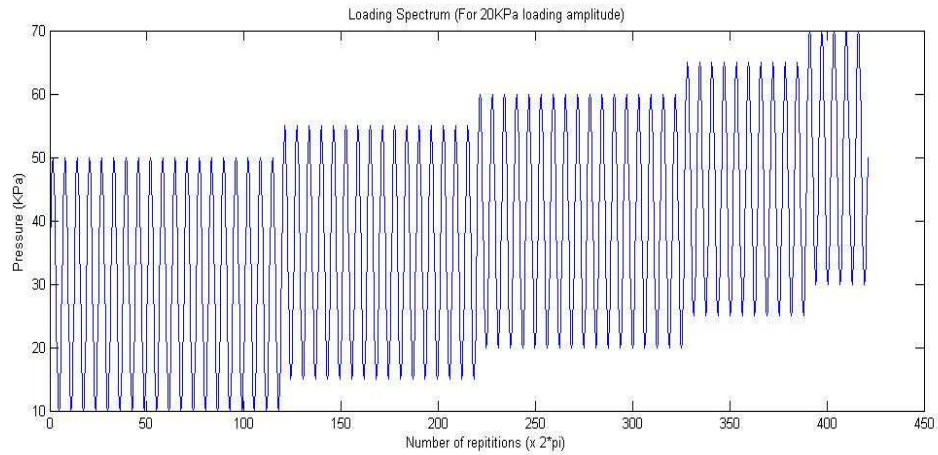
Figure 3.11: Loading Spectrum for constant amplitude

In figure 3.10, the loading spectrum with a mean of 40KPa is shown. From this figure it has been revealed that the loading ratio will vary from about 0.1 to 0.8. But lower loading ratio will have fewer repetitions. In figure 3.11, varying mean was illustrated with same amplitude.

45

4.   FINITE ELEMENT MODELING

4.1   Geometrical Modeling

The blade geometry was developed created in ANSYS using the bottom-up solid modeling method. This method requires key points to be defined first, and then lines connecting key points, to areas bounded by the lines, to finally volumes created by the surrounding areas.   The foil coordinates (x, y) were taken from previous study on structural blade design using DesignFoil [11]. Each set of foil points were fitted with splines, enclosing the foils. The sectional data are shown in table 4.1.

Table 4.1: Sectional data of the blade geometry

Station	l/L	l [m]	r [m]	c [mm]	t [mm]	t/c [%]
1	0.2	0.6	0.975	500	205	41
2	0.3	0.9	1.275	480	182.4	38
3	0.4	1.2	1.575	460	156.4	34
4	0.5	1.5	1.875	430	133.3	31
5	0.6	1.8	2.175	390	105.3	27
6	0.7	2.1	2.475	330	75.9	23
7	0.8	2.4	2.775	260	46.8	18
8	0.9	2.7	3.075	200	32	16
9	1	3	3.375	180	28.8	16

The internal geometry created (Figure 4.1) defines the skin and web thicknesses, where the remaining area is occupied by the core material. The web was created normal to the chord; therefore, a temporary chord line was drawn from the 30% cord point to the

trailing edge key point. Then for the web, four corner key points were created at the point normal to the chord line where the web connected to the skin.

The next step was to create the areas that connect one station to another, which is called skinning in the ANSYS Main Menu. Once all the areas were skinned, the final step in model generation was performed; which is the creation of volumes. Three inner volumes were created for this along with one outer shell. The inner volumes were filled up with core material. The sectional volumes are shown from figure 4.1 to 4.3.
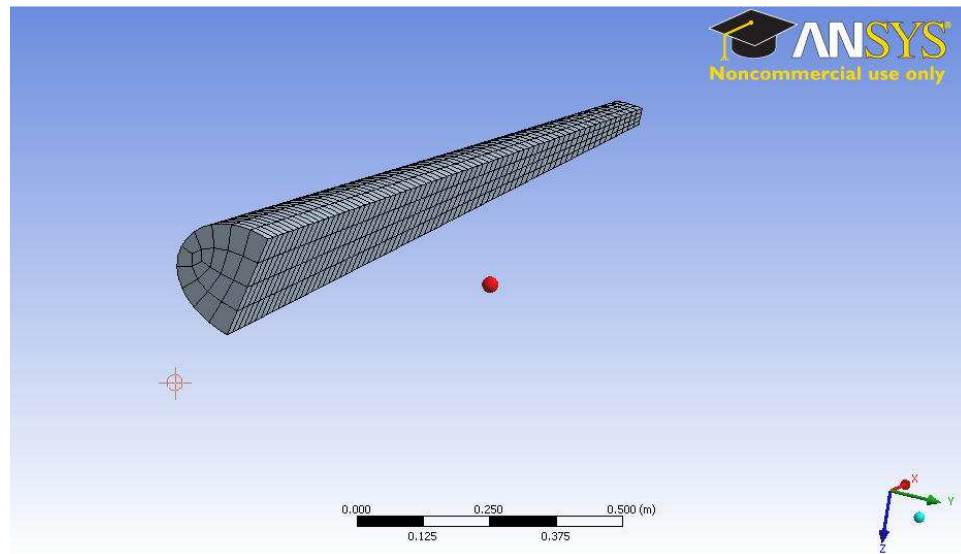
Figure 4.1: Core near the leading edge
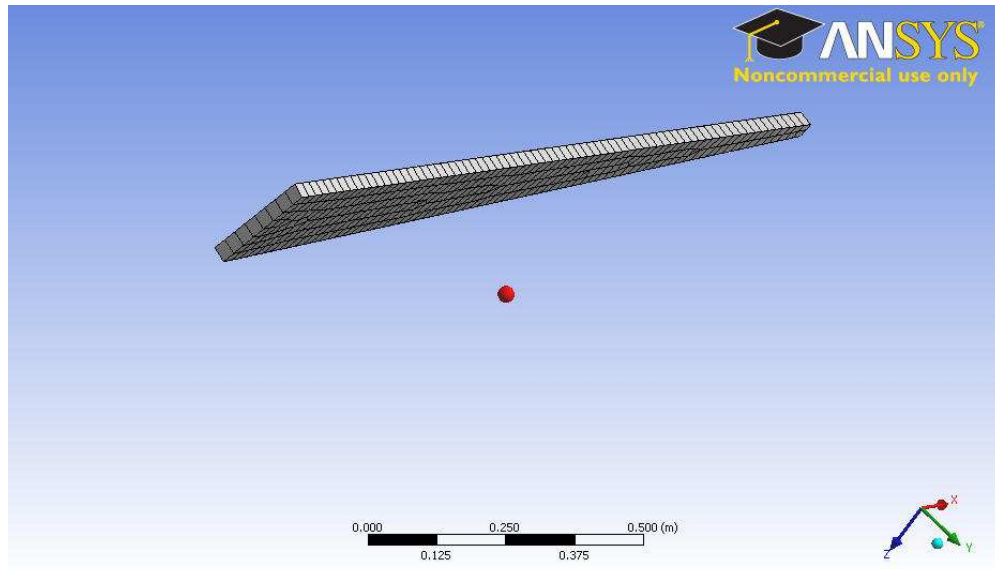
Figure 4.2: Web Support at 30% chord length
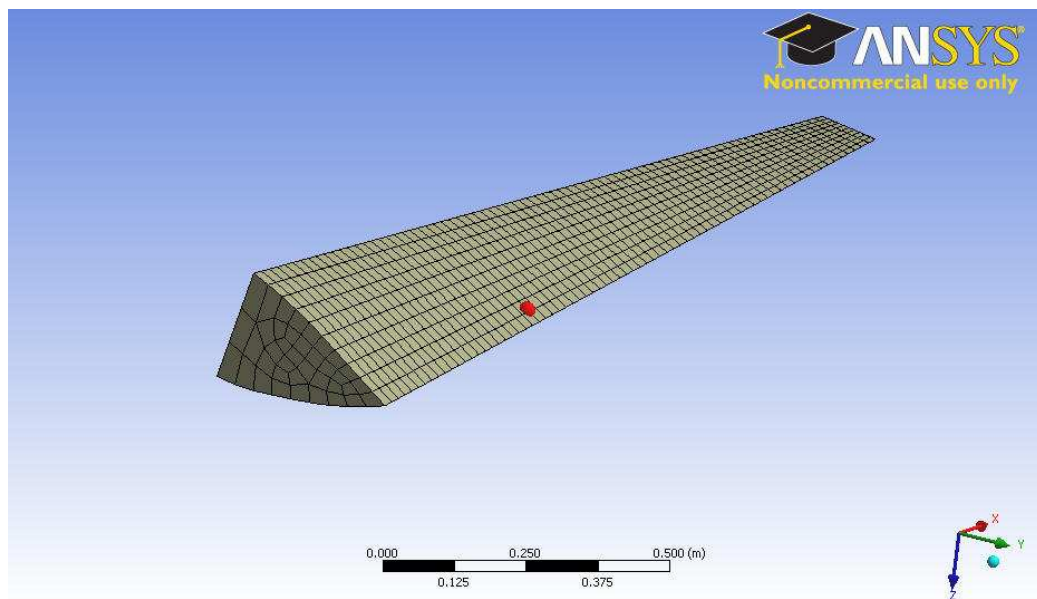
Figure 4.3: Core near the trailing edge

In the next step, the geometry created in ANSYS was transferred to ANSYS Workbench for fatigue analysis. In ANSYS Workbench, surfaces from edges were created which

could be used as outer hydrodynamic skin for the structure. The skin and the overall

blade model are shown in figure 4.4 and 4.5, respectively.
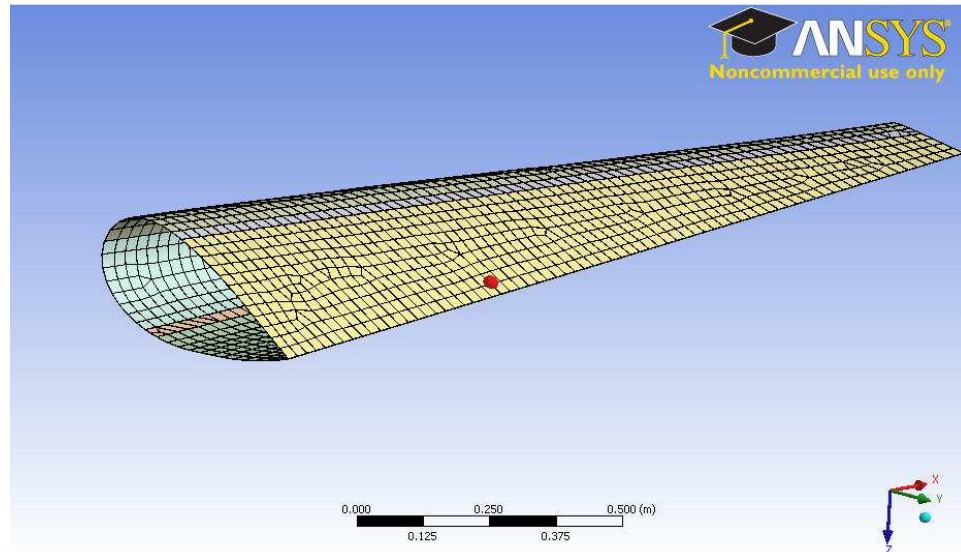
Figure 4.4: Outer shell for hydrodynamic shape
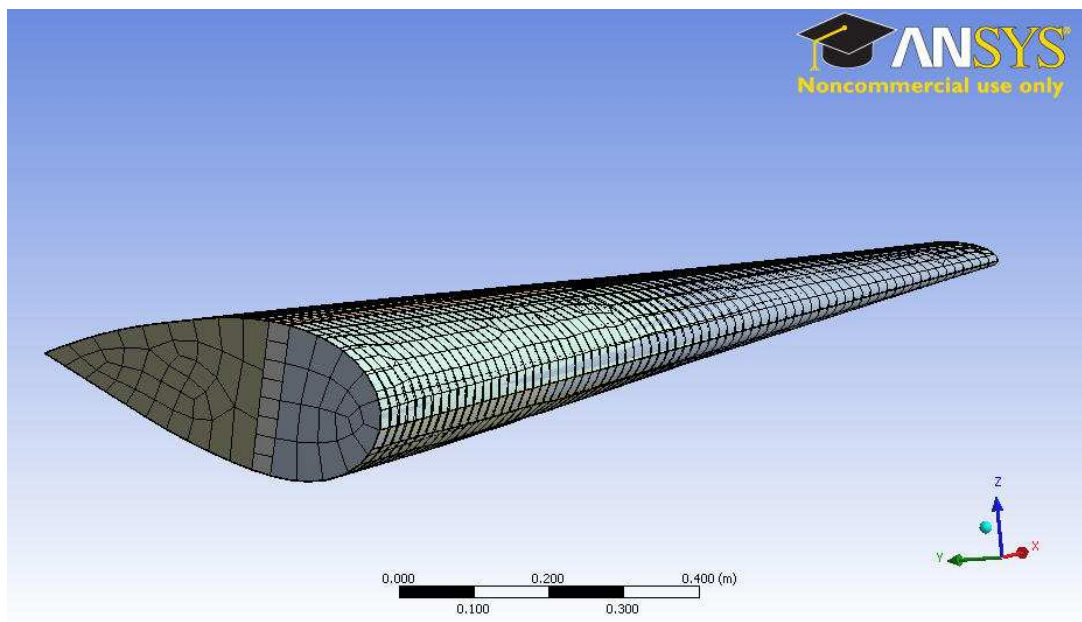
Figure 4.5: The blade with core, web support and skin

49

4.2   Element Selection

For the sandwich construction different elements were used. For core materials SOLID186 was used. For web support SOLSH190 and for outer shell SHELL181 was used. An adhesive layer was required to construct a sandwich construction. In our model CONTA174 and TARGE170 were used as interface element. The details of the elements are discussed in the following sections.

4.2.1   SOLID186 for Core Materials

SOLID186 [39] Structural Solid is well suited to modeling irregular meshes (such as those produced by various CAD/CAM systems). It is a higher order 3-D 20-node solid element that exhibits quadratic displacement behavior. The element is defined by 20 nodes having three degrees of freedom per node: translations in the nodal x, y, and z directions. The element supports plasticity, hyper elasticity, creep, stress stiffening, large deflection, and large strain capabilities. It also has mixed formulation capability for simulating deformations of nearly incompressible elastoplastic materials, and fully incompressible hyper elastic materials. The geometry, node locations, and the element coordinate system for this element are shown in figure 4.6.
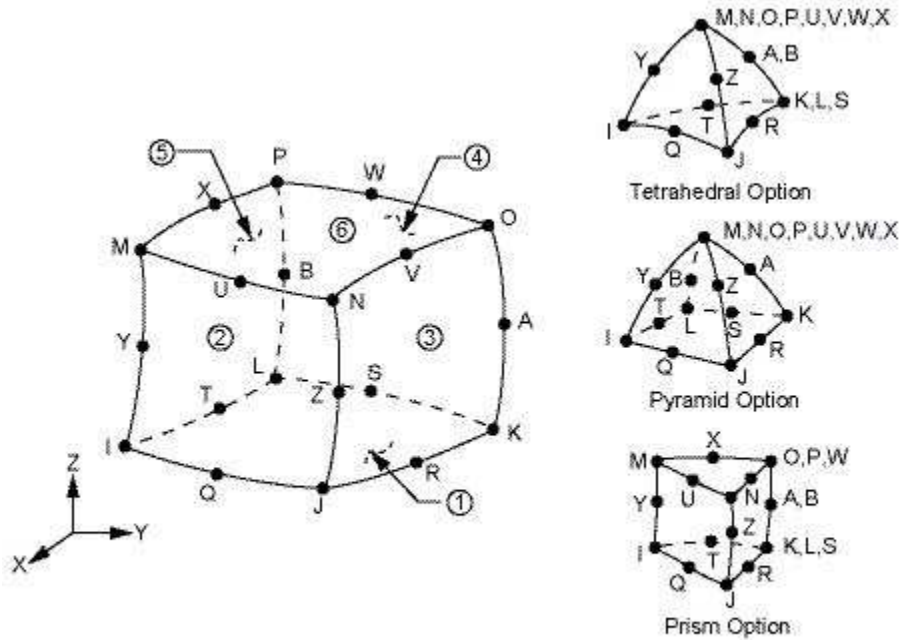
Figure 4.6: SOLID186 element geometry

As seen in figure 4.6, a prism-shaped element may be formed by defining the same node numbers for nodes K, L, and S; nodes A and B; and nodes O, P, and W. A tetrahedral-shaped element and a pyramid-shaped element may also be formed as shown in figure 4.6. In our model tetrahedral option was used. Pressures were introduced as surface loads on the element faces. Pressured were taken as positive as they acted into the element.

4.2.2   SOLSH190 for Web Support

SOLSH190 [39] is used for simulating shell structures with a wide range of thickness (from thin to moderately thick). The element has the continuum solid element topology and features eight-node connectivity with three degrees of freedom at each node: translations in the nodal x, y, and z directions. Thus, connecting SOLSH190 with other continuum elements requires no extra efforts. The element has plasticity, hyper

elasticity, stress stiffening, creep, large deflection, and large strain capabilities. It also has mixed up formulation capability for simulating deformations of nearly incompressible elastoplastic materials, and fully incompressible hyper elastic materials. The element formulation is based on logarithmic strain and true stress measures.

SOLSH190 was used for composite laminated web support. The element allows up to 250 different material layers. The geometry and co-ordinate of the element is shown in figure 4.7.
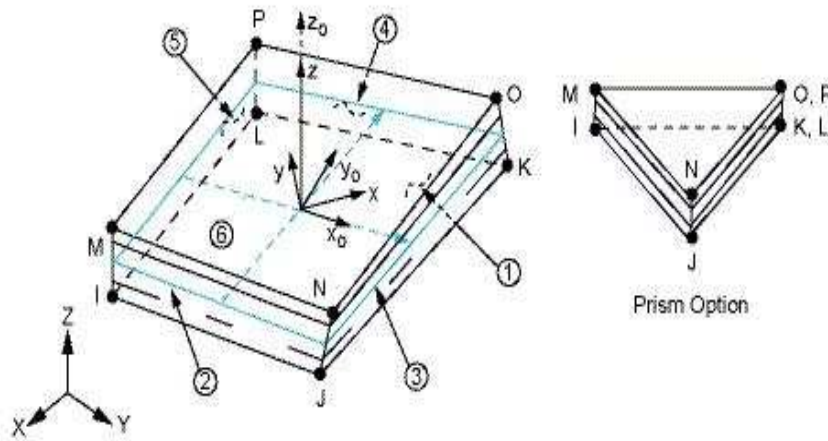
Figure 4.7: Geometry of SOLSH190 (used for Web Support)

4.2.3 SHELL181 for Outer Shell

SHELL181 [39] is suitable for analyzing thin to moderately-thick shell structures. The element kinematics allow for finite membrane strains (stretching). It is a 4 node element with six degrees of freedom at each node: translations in the x, y, and z directions, and rotations about the x, y, and z-axes. (If the membrane option is used, the element has translational degrees of freedom only). SHELL181 is well-suited for linear,

large rotation, and/or large strain nonlinear applications. Change in shell thickness is accounted for in nonlinear analyses. In the element domain, both full and reduced integration schemes are supported. SHELL181 accounts for follower (load stiffness) effects of distributed pressures. SHELL181 may be used for layered applications for modeling laminated composite shells or sandwich construction. The element configuration has been shown in figure 4.8.
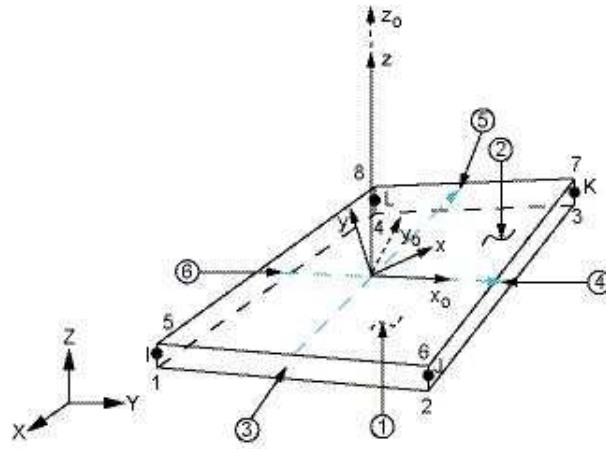
Figure 4.8: Geometry of SHELL181 element used for outer shell.

4.2.4   SOLID SHELL Contact

For constructing sandwich composite an adhesive layer between skin and core is required. For finite element analysis a contact element and a target element were used as mentioned earlier. The contact between composite outer shell and inner core as well as contact between web support and inner core was performed by using CONTA174 and TARGE170 elements.

CONTA174 is used to represent contact and sliding between 3-D "target" surfaces TARGE170 and a deformable surface, defined by this element. The element is applicable

to 3-D structural and coupled field contact analyses. This element is located on the surfaces of 3-D solid or shell elements with mid-side nodes (SOLID95, SOLID98, SOLID122, SOLID123, SOLID186, SOLID187, SOLID191, SOLID226, SOLID227, SOLID231, SOLID232, VISCO89, SHELL91, SHELL93, SHELL99, SHELL181, SHELL281, and MATRIX50). It has the same geometric characteristics as the solid or shell element face with which it is connected as shown in figure 4.9. Contact occurs when the element surface penetrates one of the target segment elements (TARGE170) on a specified target surface.
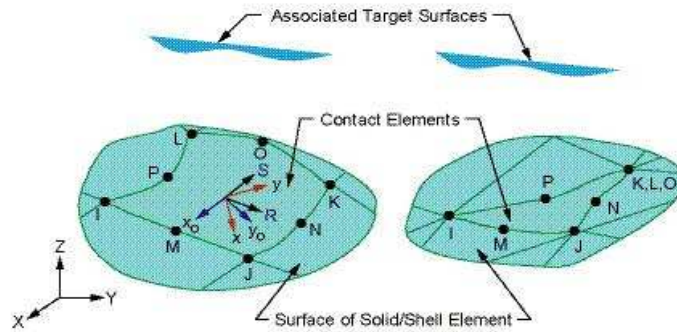
Figure 4.9: Element Geometry of CONTA174

TARGE170 is used to represent various 3-D "target" surfaces for the associated contact elements (CONTA173, CONTA174, CONTA175, CONTA176, and CONTA177). The contact elements themselves overlay the solid, shell, or line elements describing the boundary of a deformable body and are potentially in contact with the target surface, defined by TARGE170. This target surface is discredited by a set of target segment elements (TARGE170) and is paired with its associated contact surface via a shared real constant set. For rigid target surfaces, these elements can easily model complex target shapes. For flexible targets, these elements will overlay the solid, shell, or line elements

54

describing the boundary of the deformable target body. The element geometry is shown in figure 4.10.
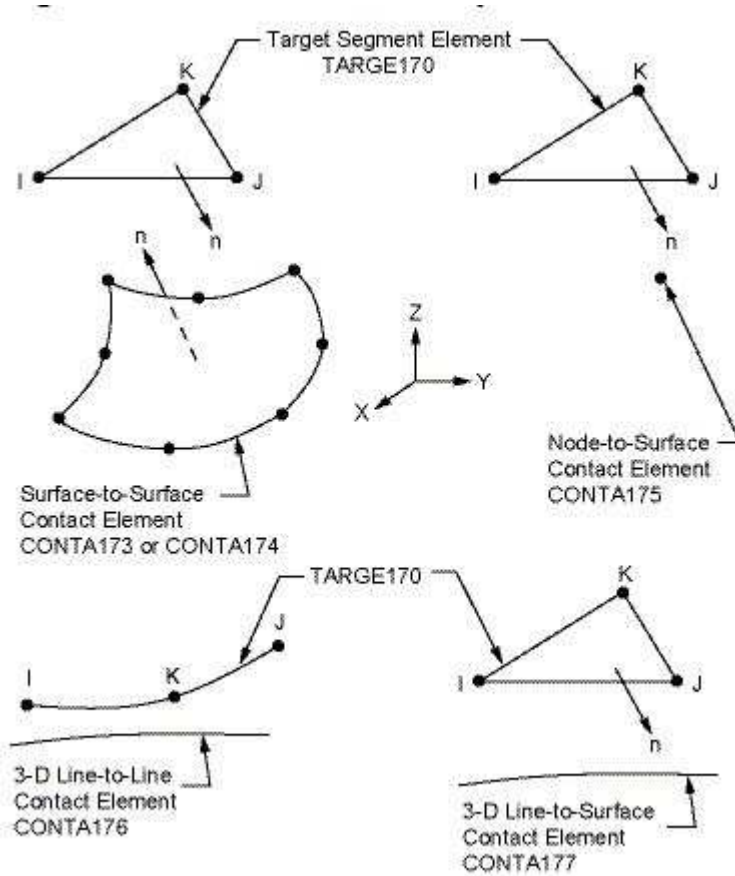
Figure 4.10: Geometry of the TARGE170 element

4.3   Materials Properties

Three different types of materials were used for this analysis. Carbon/Epoxy was used for the outer shell. Glass/Epoxy was used for web support and Divinycell HC100 was used for core. The material properties and layer orientation of the composites are shown in table 4.2-

Table 4.2: Material Properties for Blade Design [34]

Materials	Outer Shell (Skin)	Web Support	Core
	Carbon/Epoxy	Glass/Epoxy	Divinycell 100 HCP
Density, ρ (kg/m^3)	1600	1970	100
Longitudinal Modulus, E_1 (GPa)	147	41	0.24
Transverse in Plane Modulus, E_2 (GPa)	10.3	10.4	-
Transverse out of Plane Modulus, E_3 (GPa)	10.3	10.4	-
In Plane Shear Modulus, G_{12} (GPa)	7	4.3	-
Out of Plane shear Modulus, G_{23} (GPa)	3.7	3.5	-
Out of Plane shear Modulus, G_{13} (GPa)	7	4.3	-
Major in Plane Poisson's ratio, υ_{12}	0.27	0.28	0.3
Out of Plane Poisson's ratio, υ_{23}	0.54	0.5	-
Out of Plane Poisson's ratio, υ_{13}	0.27	0.28	-
Lay up Sequences	$[(-+45)_2 0_6]_s$	$[(-45)_6/(+45)_6]_s$	-
Thickness of layer	0.5 mm	0.5 mm	-

4.4   Mesh Generation

The meshing of the turbine blade started with the webs. The layered elements were given a stacking sequence. A single element represents the laminate thickness. Therefore, the webs were set with one element division. The webs were meshed with volume mapped hexahedrons, using the mesh tool in the GUI. The skin was created from the edges. Shell 181 elements were used to mesh the outer skin. The core was meshed with SOLID 186 element as stated above. All meshing performances were performed

using GUI command. A contact and target elements were applied in between core and skin interface. The meshed volume is shown in figure 4.11.
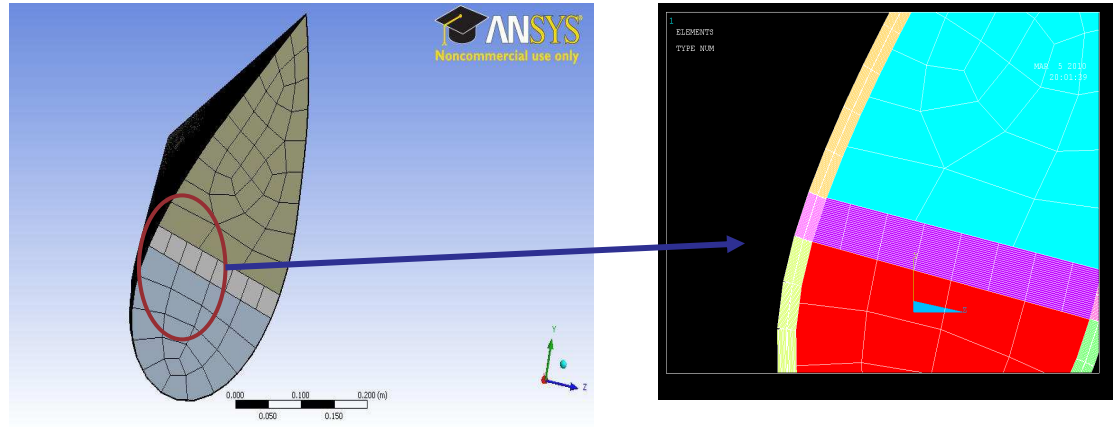
Figure 4.11: Meshed blade (Left) and a close view of the skin and foam (Right)

4.5   Static Analysis

First a static analysis was performed to compare the modified design with previously designed blade by Asseff, N. and Mahfuz, H. [11]. Static analysis was also necessary to calculate ultimate strength of the blade and also to locate the critical zone for fatigue analysis. The blade was considered as a cantilever beam. The root of the blade was fixed in all directions. The flapwise pressure distribution was applied to the low pressure side as surface loads. The negative pressures are applied using the SFA command. The pressures were transferred by default from the geometry to FE model, where they were applied to the skin element. The fixed support and the loading are shown in the figure 4.12.
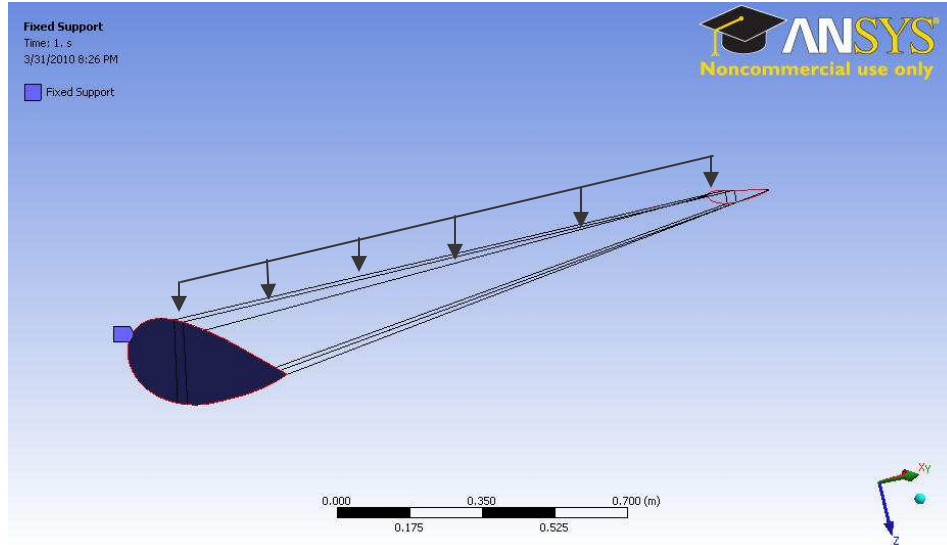
Figure 4.12: Boundary conditions and loading

The bending stress, interlaminar shear stress and deformation of the blade has been determined and compared with previous results.

4.6   Fatigue Analysis

For damage calculation due to fatigue loads, an S-N diagram was developed using ANSYS Workbench's special feature Fatigue Tool. Fatigue loads have been imposed on the OCT blades to determine the fatigue cycles. There are essentially four classes of fatigue loading-

- Constant amplitude, proportional loading

- Constant amplitude, non-proportional loading

- Non-constant amplitude, proportional loading

- Non-constant amplitude, non-proportional loading

As OCT blade will be subjected to non-constant amplitude loading, stress analysis from this type of loading require a specific loading distribution or loading spectra. Loading

spectra calculated in the previous chapter was considered for compatibility. From these random loading histories different stress amplitudes were found. These different stress amplitudes i.e. stresses were used to determine the fatigue cycles.

The steps involved for constructing the S-N diagram is shown in figure 4.13.

```
                    ┌──────────────────────┐
                    │   Initial Loading    │
                    │                      │
                    │                      │
                    └──────────┬───────────┘
                               │
                               ▼
                    ┌──────────────────────┐
                    │   Stress Analysis    │
                    └──────────┬───────────┘
                               │
                               ▼
                    ┌──────────────────────┐
          ┌────────►│       n + ∂n         │
          │         │   n= Initial cycles  │
          │         │ ∂n= Increment of Cycles │
          │         └──────────┬───────────┘
          │                    │
     NO   │                    ▼
          │            ╱ Safety Factor ╲
          └───────────    And
                          Failure
                       ╲   Check    ╱
                               │
                              YES
                               ▼
                    ┌──────────────────────┐
                    │  Fatigue Cycles (Nf) │
                    └──────────────────────┘
```
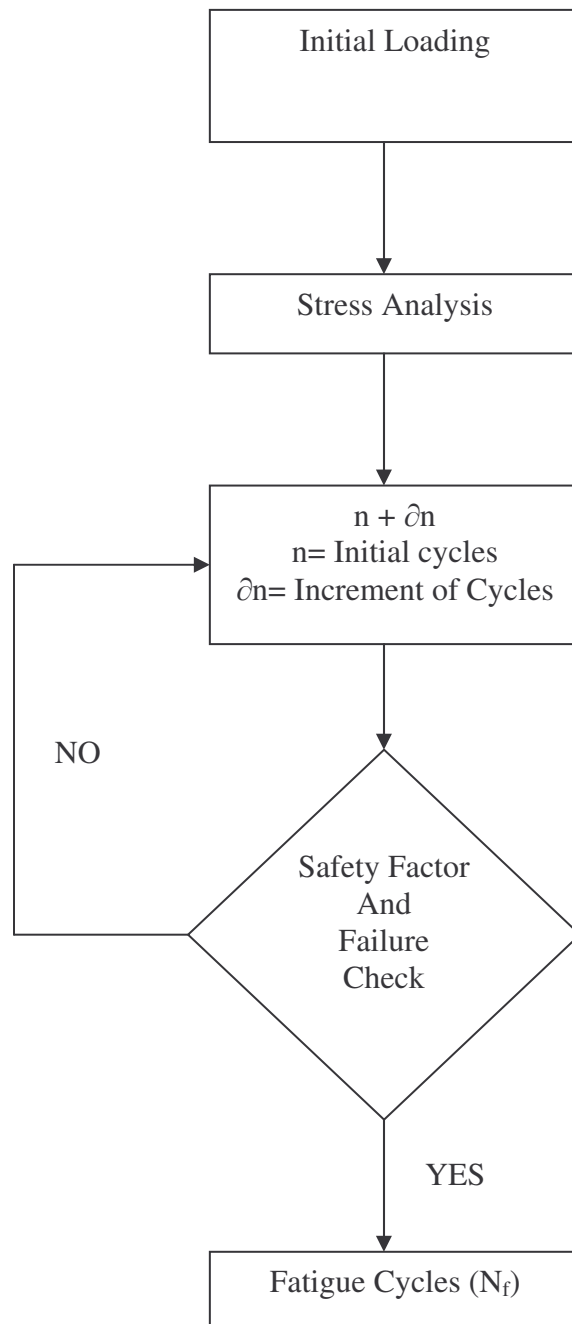
Figure 4.13: Steps involved for developing S-N diagram in ANSYS.

Based on loading history and ultimate strength, four different loading events were performed. It was mentioned that there was a feature in ANSYS which could use the random loading as input. These random loading could create alternating bending stress and shear stress on the blade. For developing an S-N diagram, constant amplitude fatigue analysis were performed. The loading events are tabulated in the table 4.3.

Table 4.3: Loading Event for S-N Diagram

Loading Event	Load (KPa)	Loading Ratio	Frequency (Hz)
1	120	0.1	1
2	105	0.1	1
3	90	0.1	1
4	75	0.1	1

From the static analysis it was revealed that safety factor at core had lower value under shear loading. It means that the core would fail first under shear loads. Therefore, shear stress was taken into account for developing S-N diagram. Safety factor was investigated after each increment of cycles. The increment was set for 1×10^5 cycles. It means that after this many cycles of loading, the factor of safety and Tsai Wu failure criteria was used to determine whether the blade has failed or not. If the safety factor dropped below 1.0 or Tsai Wu Index exceeded 1.0 then the loading was stopped. But in all four cases it was been found that safety factor was dropped below 1.0 before the Tsai Wu failure index exceeded 1.0.

5.   RESULTS AND DISCUSSION

5.1   Effect of varying loads on Turbine Blades

Turbine blade will be subjected to fatigue loads originated from different sources as discussed in section 3.4. Previously detailed in chapter 3, the varying loads on OCT blade will cause alternating bending and shear stress. The effects of varying loads on the development of stresses in the blade are discussed in the following sections. Numbers of repetition of stresses with specific amplitudes were determined using Rain flow Counting Method.

5.1.1   Effect on Bending Stress

During operation of the turbine blade, the amplitude of loading will not be constant but it will experience varying alternating loads with a mean of 40KPa and a standard deviation of 12KPa. These varying alternating loads will create alternating bending stress of 1MPa to 40MPa from a mean bending stress 40.1MPa. This bending stress was examined for 0° ply at high pressure side. Maximum bending stress was found for this fiber orientation in hydrodynamic skin from the static analysis. The variation of alternating bending stress is shown in figure 5.1. Number of repetitive stress cycles determined from this figure. It also reveals that higher alternating bending stress has lower number of repetition.
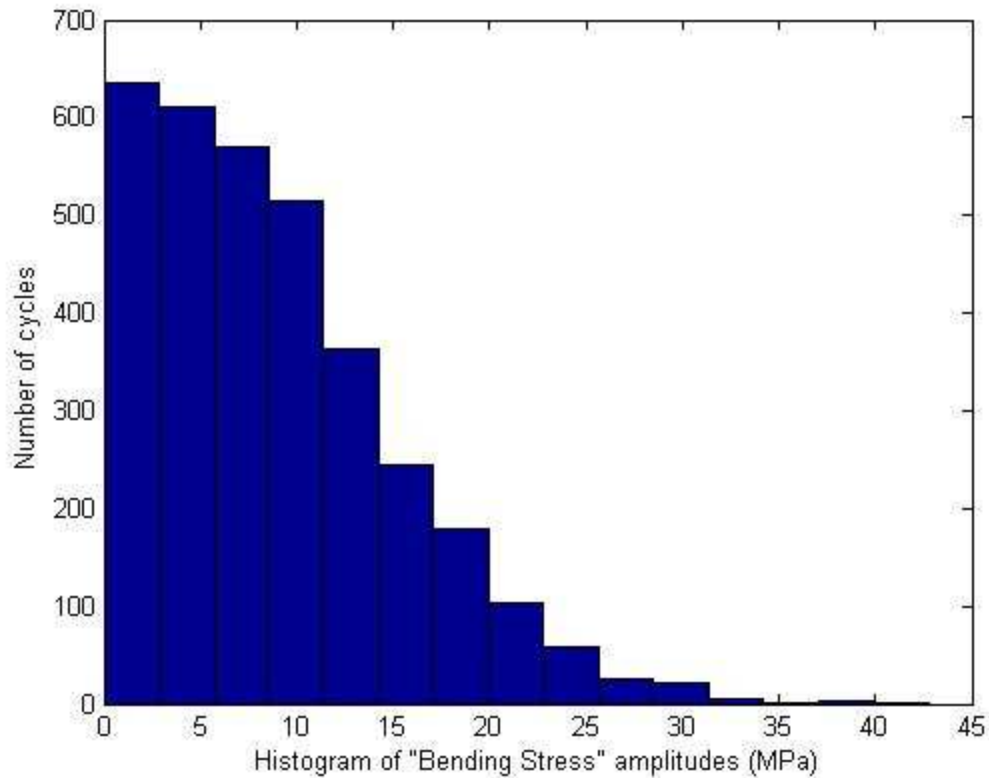
Figure 5.1: Varying alternating bending stress due to varying alternation loads.

5.1.2 Effect of Core Shear Stress

For sandwich composite shear stress of core is more important than the bending stress as sandwich composite mostly fails by core shear. Hence effect of varying alternating loads on core shear stress was analyzed. This stress was examined at core near the root. 400 elements were investigated near the root of the blade at section 1. The effect of alternating loads on core shear stress is illustrated in figure 5.2 where it demonstrates that the amplitude of core shear stress will vary from 0 to 0.57MPa. The amplitudes of these loading have a mean of 0.51MPa. It is noted that 'stress level' is the sum of mean and alternating stress. So, the stress level will vary from 0.51MPa to 1.08MPa. From the figure it is clear that the blade will experience higher stress level for fewer times.
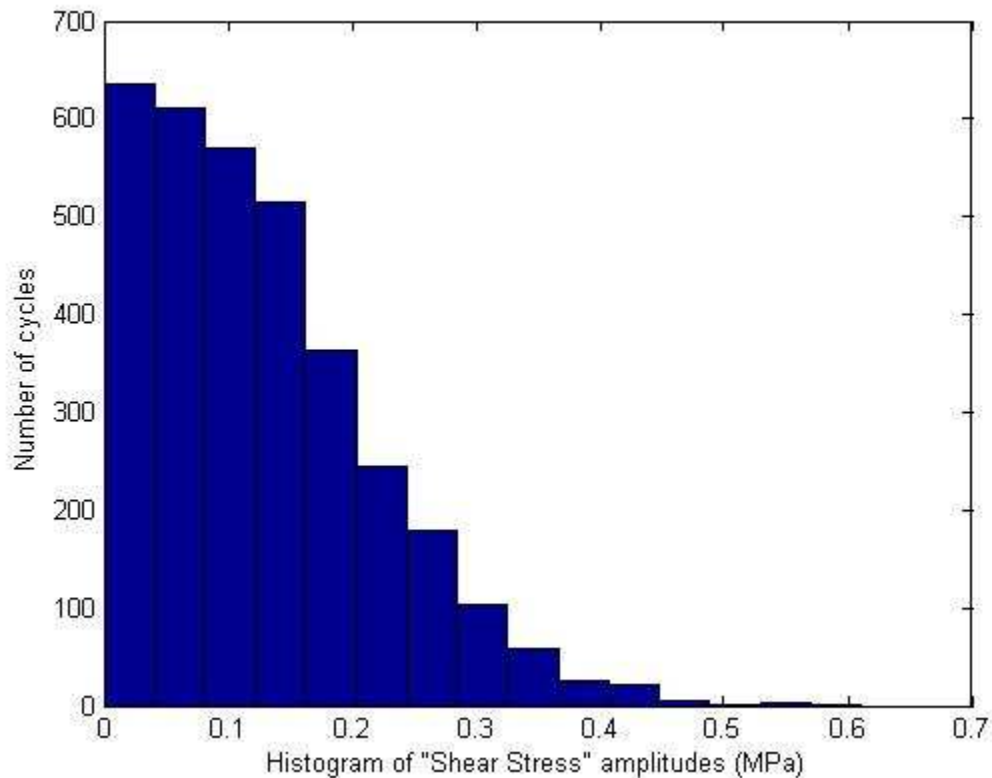
Figure 5.2: Varying alternating shear stress due to varying alternation loads.

5.2   Static Analysis using ANSYS

5.2.1   Static Analysis for one web support

The design of the blade was modified from the previous study by considering one web support instead of two. From static analysis it is observed that use of one web at 30% chord length is much stiffer than the use of two webs. The maximum deflection is found at the tip and it was 15.0 mm which is 5 mm less than the previous studies. The deflection of the blade is shown in figure 5.3. Also the maximum bending stress at skin is lower than the previous study by 17.2 MPa. The maximum bending stress is shown in figure

64

5.4. Maximum bending stress was found in the skin composite near the root. Hence, using one web support is advantageous from mechanical as well as economical point of view as it will reduce cost of web materials.
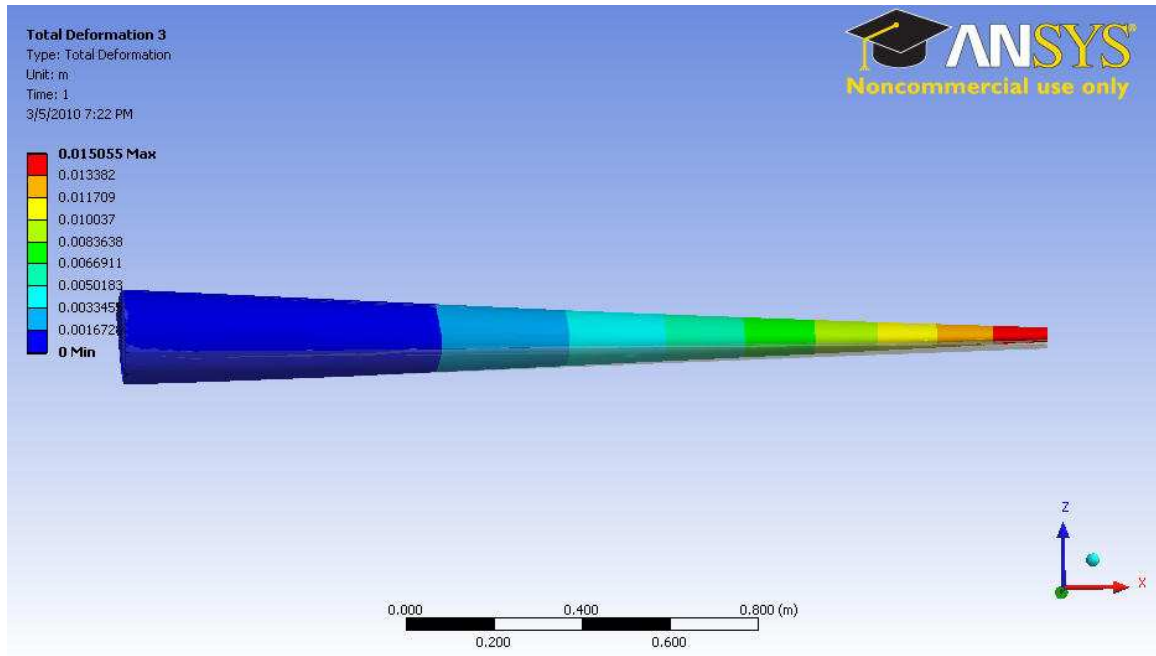
Figure 5-3: Deflection of the blade due to static load
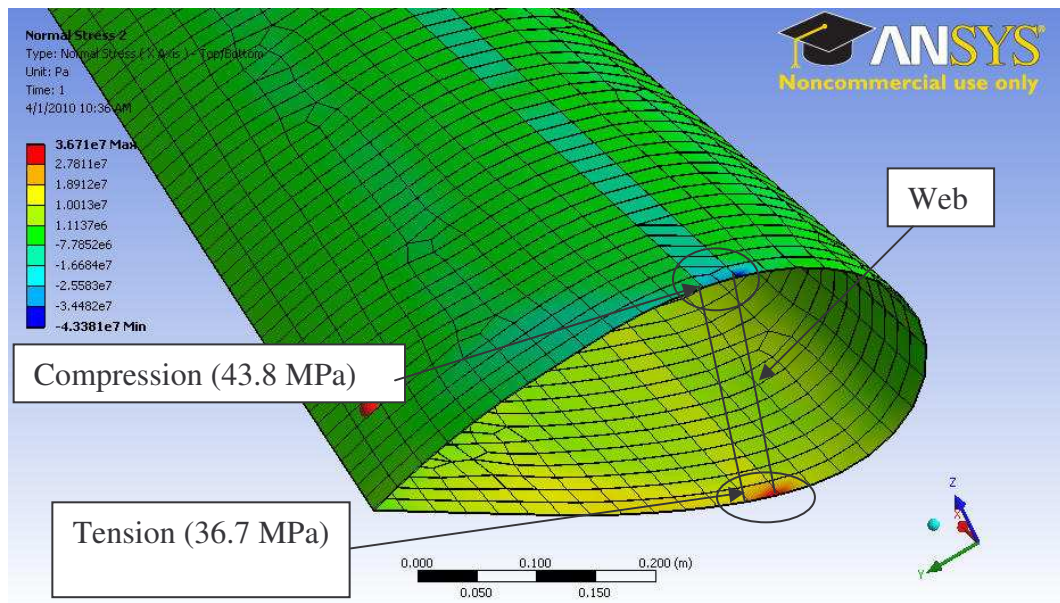
Figure 5.4: Maximum bending Stress at outer skin near the root and web support

It is observed in figure 5.4 that the bottom skin will be in tension and top skin is in compression. This is due to cantilever beam effect. When the blade is under load it bends in the direction of the lift forces causing the low pressure side to be in compression while the high pressure side is in tension. This trend is illustrated in figure 5.5 below.
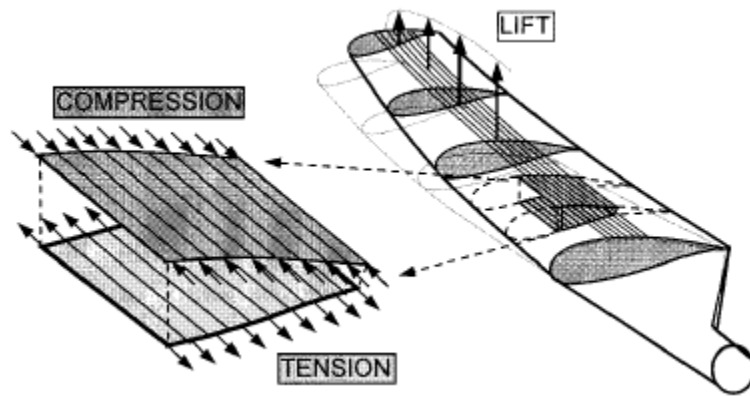
Figure 5.5: Schematic showing loads resulting in tension and compression [11]

Bending stresses along the length was also examined. Unlike the previous design [11], there was no stress concentration due to ply drop. In previous design, there were drop of some plies to accommodate two web supports. But in current design ply drop was not required as only one web support was used. Bending stresses along the length of the blade is shown in figure 5.6 below-
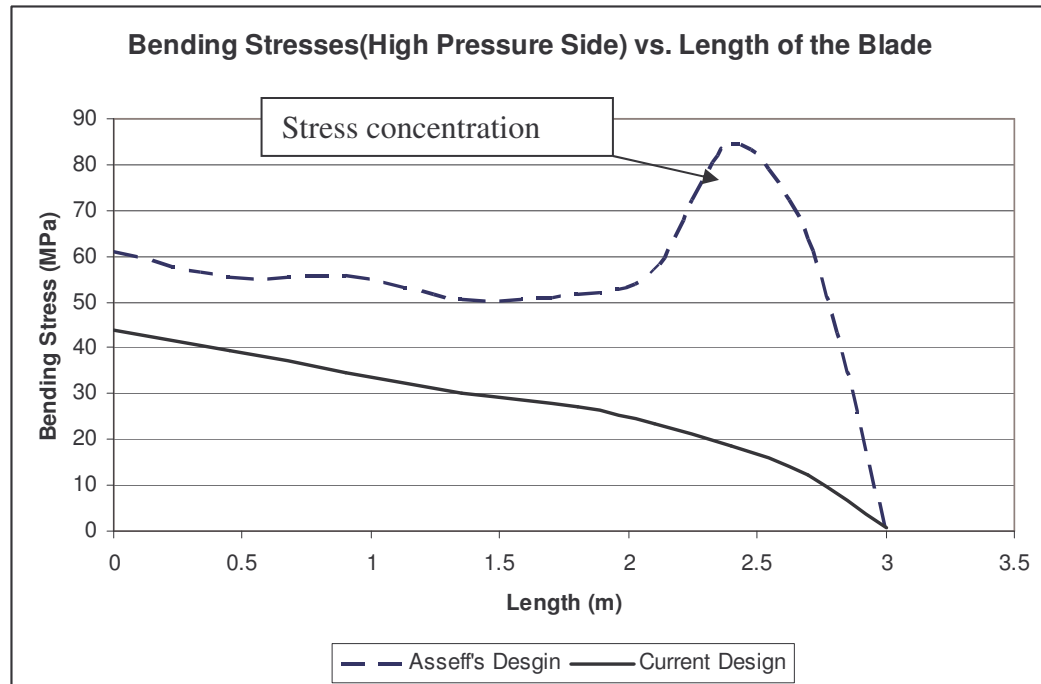
Figure 5.6: Bending stresses (Compressive at High Pressure Side) along the blade

In this figure it was clear that there would be no stress concentration for current design. In previous design by Asseff, N., there was an irregularity in geometry near the tip i.e. 2.5m form the root of the blade due to ply drop. Any irregularity could create stress concentration which can alter the fatigue behavior. The bending stress for layer number 6 was investigated.

The comparative studies between two designs are tabulated in Table 5.1.

Table 5.1: Comparison of two designed OCT blade

	Current Design	Previous Design
Number of Webs	1	2
Position of Web Support (%of Chord Length)	30% (From Leading Edge)	25 % and 75% (From Leading Edge)
Maximum Deflection (mm) Maximum Bending Stress (Mpa)	15.01 (At tip) 43.8 (Near Root) (Layer 6, 0°)	20.01 (At tip) 61.1 (Near Root) (Layer 6, 0°)

5.2.2 Static Analysis for Ultimate Loading

Static test was performed to extract relevant load levels for developing S-N diagram using ANSYS. An incremental load 5KPa was used. Von Mises failure criteria for foam core and Tsai Wu criteria for skin and web support were examined simultaneously.

With increasing load, the development of stress would increase. As Failure Index associated with Tsai Wu criteria is directly proportional to the development of stresses in composites. Therefore, Tsai Wu index was increasing with the increment of applied load. On the other hand, Safety factor related with Von Mises failure is inversely proportional to the development of von mises stress. As a result, this safety factor for foam core was decreasing with the applied load. The change of safety factor and failure index with respect to applied loads is shown in figure 5.7.
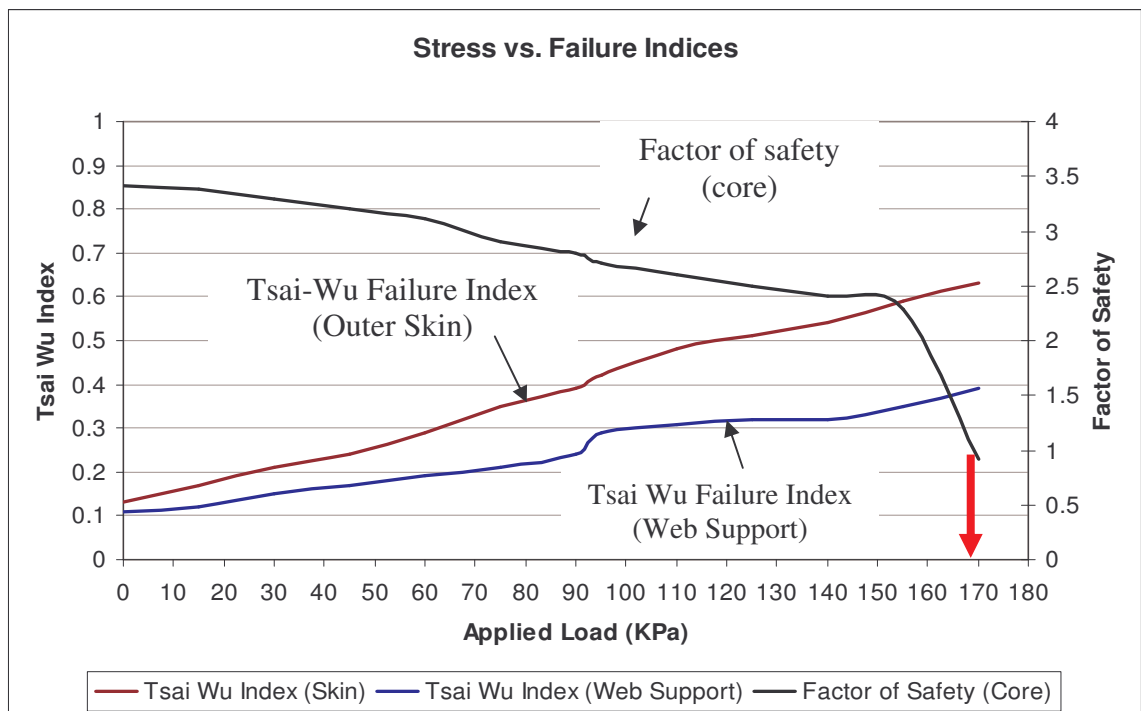
Figure 5.7: Static Analysis for Ultimate Loading

From this figure it has been found that the blade could withstand up to 170KPa load. At this load safety factor at core near the root dropped below 1.0. But the composite could take more loads. The shear stress and bending stress in foam core near the root was found 1.40MPa and 2.56MPa respectively under this ultimate load. The safety factor for foam core and maximum failure index for composites are shown from figure 5.8 to 5.10. From this analysis it is clear that the blade would fail at foam core at root. Therefore, fatigue analysis is performed based on the developed stress at foam core.
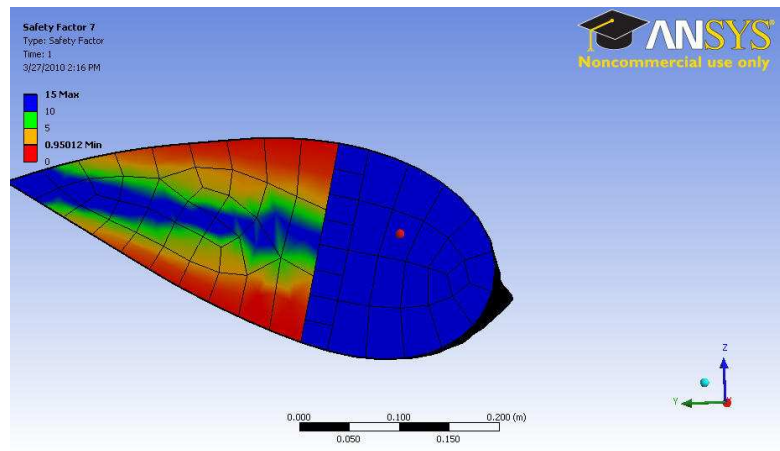
Figure 5.8: Safety Factor (core) near the root at ultimate loads
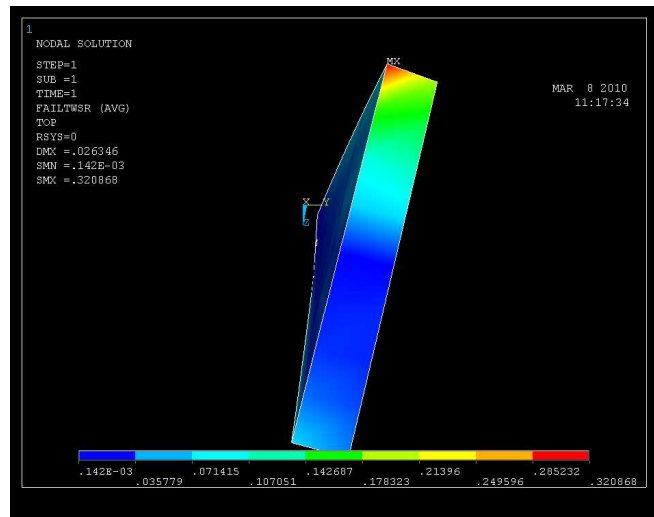
Figure 5.9: Tsai Wu Failure Index (web support) at ultimate load
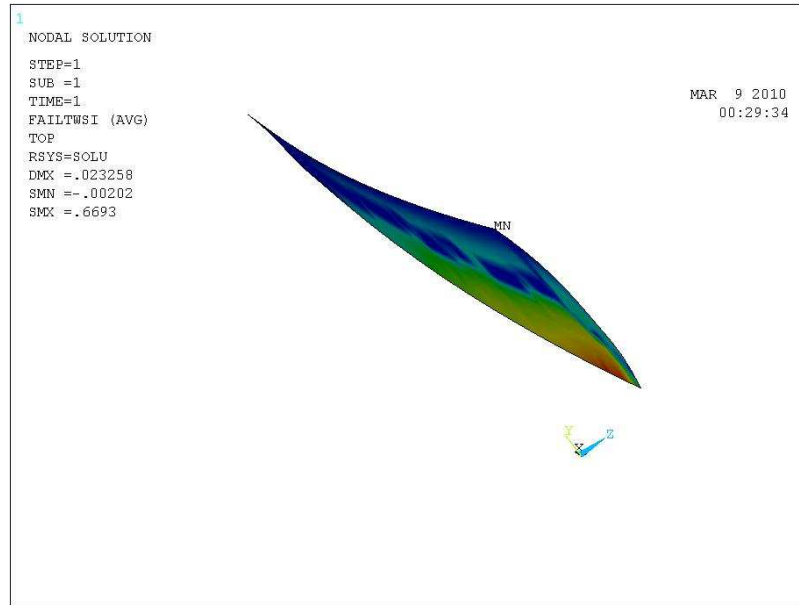
Figure 5.10: Failure Index (High Pressure Side, Layer 6) at ultimate load

5.3   Fatigue Analysis

After determining the strength of the blade four loading events were considered for fatigue analysis. The loading events are tabulated in table 5.2. In each case, factor of safety and Tsai Wu Index was checked for determining the cycles to fail. From Rainflow Counting Algorithm it was observed that the loading ratio will vary from 0.1 to 0.8. Effect of loading ratio on fatigue behavior is shown in figure 5.11.

70
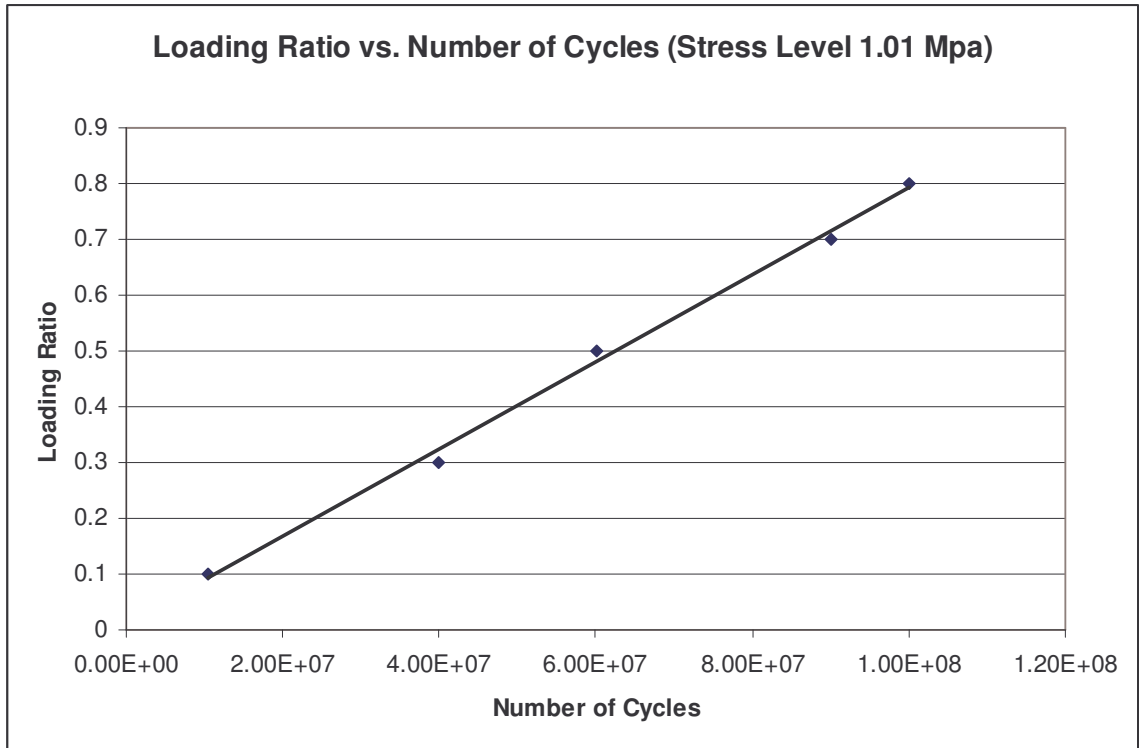
Figure 5.11: Effect of loading ratio on fatigue cycles

From the above figure, it was clear that higher loading ratio had longer life cycles. Therefore, lower for a conservative design, a lower loading ratio was used. The maximum number of load cycles was set at 1×10^8 cycles. After the completion of these cycles it was assumed that the blade would not fail due to fatigue. Figure 5.12 shows the data generated for S-N diagram. From this diagram, fatigue strength was found to be at 48% of the ultimate shear strength of core.

Table 5.2: Loading event and fatigue cycles

Loading Event	Applied Load (% of ultimate load)	Loading Ratio	Stresses at core (near the root)	
			Shear Stress (% of ultimate strength)	Bending Stress (%of ultimate strength)
1	120(70%)	0.1	1.01(64%)	2.25 (65%)
2	105(61%)	0.1	0.9(57%)	2.13 (61%)
3	90(52%)	0.1	0.8(51%)	2.05 (59%)
4	75(43%)	0.1	0.7(46%)	1.91 (55%)
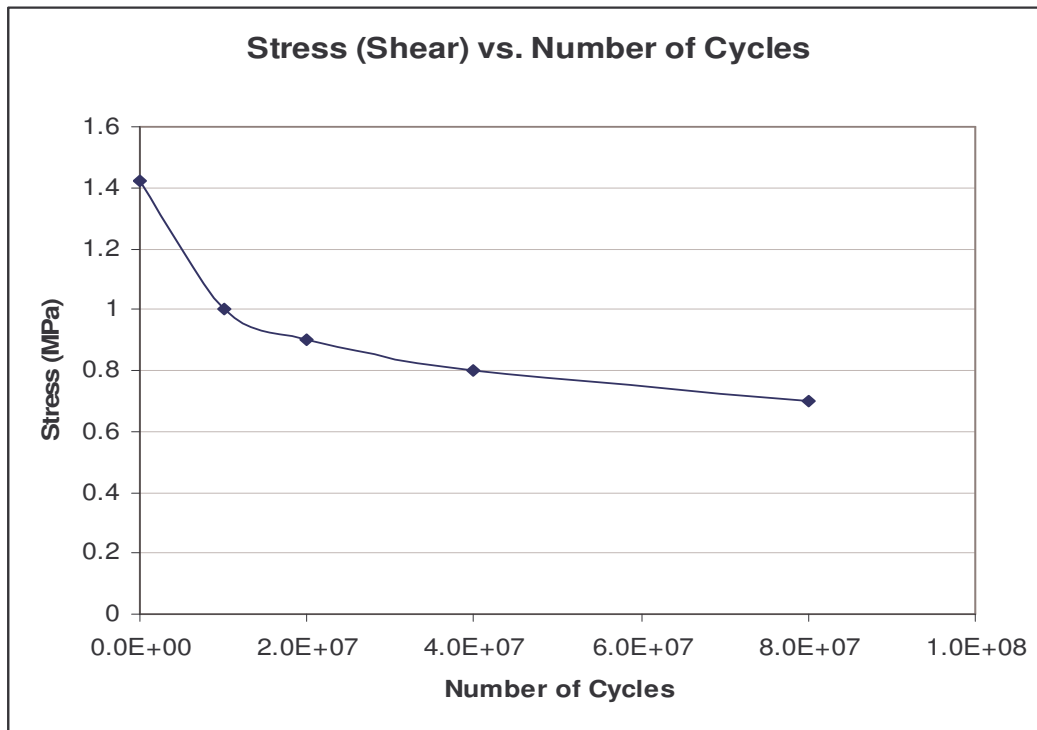
Figure 5.12: S-N diagram (Frequency 1 Hz and Loading Ratio 0.1)

5.4 Safety Factor Analysis

Safety factors of the blade were investigated under shear stress levels. These safety factors were examined after 10^5 cycle's interval. Safety factor is related with the strength of the blade as discussed in chapter 2. ANSYS uses the degradation of material's

strength with the increase of load cycles. The degradation is very low and it follows almost linear degradation. So with the increase in number of cycles the safety factor decreased as discussed earlier in failure theory. But near the very end of the fatigue cycle the safety factor decreased very rapidly meaning that the damage of the blade was catastrophic.

One loading event is shown here with stress level 1.01MPa, loading ratio 0.1 and a loading frequency of 1 Hz. The safety factor dropped below 1.0 after 1.05×10^7 numbers of cycles. The variation of safety factors with number of cycles is shown in figure 5.13. From this figure it is observed that the rate of degradation of material strength is almost linear as ANSYS uses, but it fails catastrophically near the very end of the fatigue life.
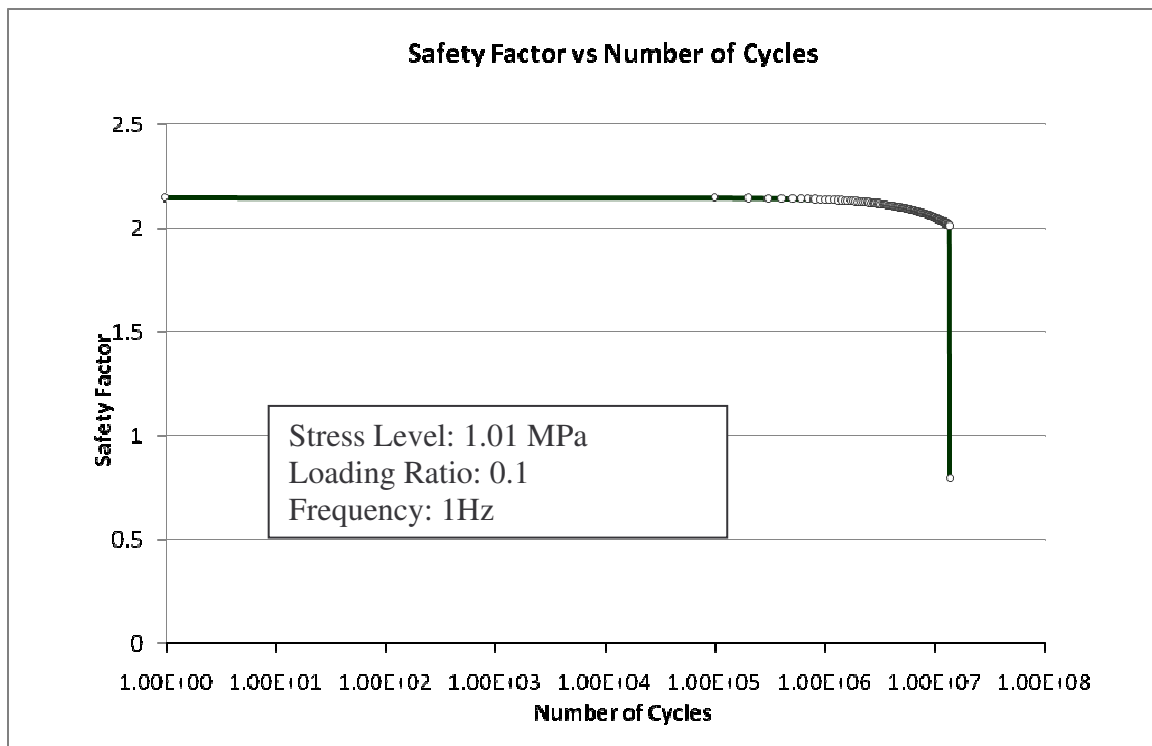
Figure 5.13: Safety Factor Analysis for determining fatigue cycles

The catastrophic failure of the blade near the very end of the fatigue life can be explained from the study made by Kulkarni et al. [40]. Though they studied for three points bending but this is more or less applicable in all loading cases for sandwich composites under flexural loading. They found three distinct damage events for sandwich composite with foam core. The damage events are shown in figure 5.14. The damage events are marked with '1', '2', and '3'.
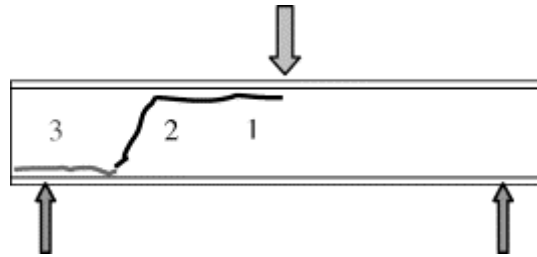
Figure 5.14: Damage Events of Sandwich Composite under Flexural Loading [34].
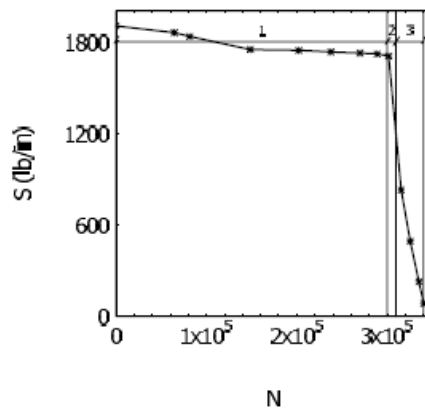
Figure 5.15: Degradation of strength of sandwich composite [34]

They found that damage event 1 occupies almost 85% to 90% of fatigue life. The degradation of strength was also shown in figure 5.15 for three different stages. The

74

sandwich fails catastrophically at the end of the fatigue life. This catastrophic failure is due to the failure of the core by shear. Safety factors before and after the last increment of load cycles is shown in figure 5.16.
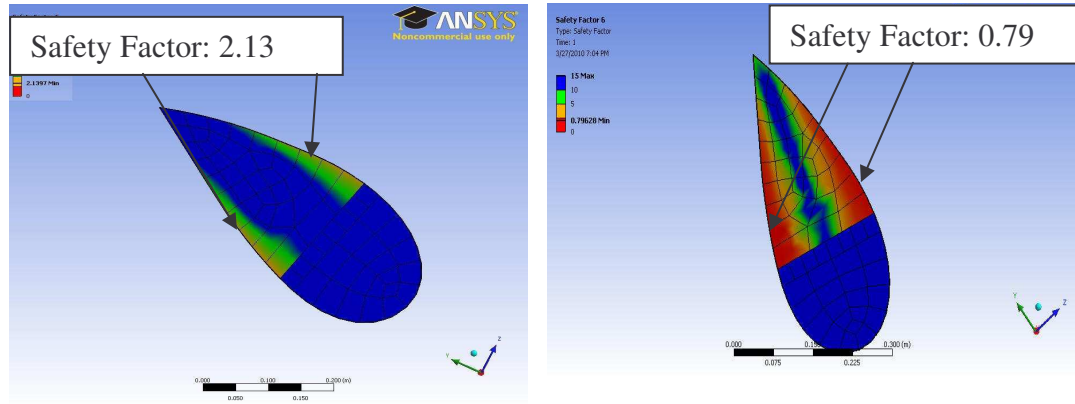
Figure 5.16: Safety factor before (a) and after (b) the last increment of load cycles

From the above figure it was clear that safety factor dropped from 2.13 to 0.79 at the very end of fatigue cycle. Safety factor did not vary at rest of the fatigue life. Kulkarni et al. found that the damage initiated below the point of applied loads. But for case it would start at the fixed end of the blade. This was due to maximum moment at the root of the blade.

5.6   Effect of Stress Level

Stress level also has an effect on damage propagation or reduction in safety factor. Although the degradation of material properties and the safety factor are linear for all stress levels but higher stress magnitude will cause a shorter lifetime. The effect of stress level on fatigue behavior is shown in figure 5.17.
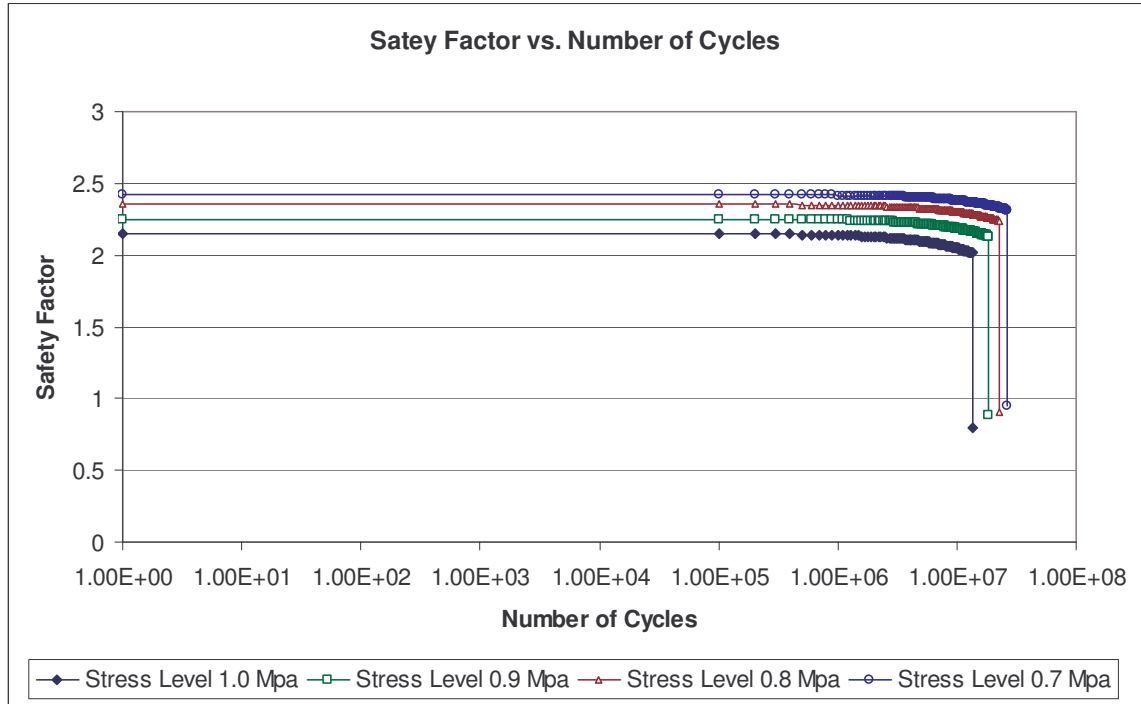
Figure 5.17: Effect of stress level on safety factors (log scale)

In figure 5.9 it was observed that shear stress magnitude with 1.01MPa i. e. 64% of ultimate shear strength had a life time of 1.05×10^7 cycles. With the decrease of stress magnitude the fatigue life cycle would increase. Run out cycle was set at 1×10^8. At 43% of ultimate load the safety factor of the blade did not drop below 1.0. It means that the blade would have an infinite life time for a load level below 75KPa. That's why no simulation was performed for shear stress level below 0.7 i.e. applied loads 75KPa.

5.7   Effect of frequency

For fatigue analysis, frequency is one of the important parameters. Loading sequences have not been considered in Palmgren-Miner's method; hence loading frequencies don't have effect on fatigue which may cause aberrant results in overall fatigue damage calculation. To examine this uncertainty, two S-N diagrams have been

developed in ANSYS with two different frequencies in order to check the variation of fatigue results. At 50m depth the loading variation would be very low. It was assumed that the loading frequency would be 1 Hz. The loading frequency could change for severe condition. But at such a high depth the possibility of severity is less. From Raye's work on velocity of the Gulf Stream current we found that variance of velocity decreased with the increase of water depth. And the turbine blade is thinking to install at 50m depth to avoid high randomness of surface ocean waves as well as severe weather conditions. Therefore it is very unlikely to repeat the load or stress cycle with higher frequencies. In this work two loading frequencies of 1 Hz and 0.5 Hz were considered for developing S-N diagrams to investigate the fatigue behavior. Failure cycles for different frequencies are tabulated in table 5.3. From this table, one could easily find negligible effect on fatigue behavior for frequency changes from 1Hz to 0.5Hz. This concept is analogous with Clerk et al. [19] studies where they mentioned that S-N diagram will be almost same for any frequency lower than 1 Hz.

Table 5.3: Effect of frequencies on failure cycles

Applied Load (KPa)	Number of failure cycles	
	Frequency	
	1Hz	0.5Hz
170	1	1
120	1.05×10^7	1.35×10^7
105	2.10×10^7	2.35×10^7
90	4.20×10^7	4.40×10^7
75	8.30×10^7	8.50×10^7

5.8   Damage Calculation

Fatigue Damage was calculated using Palmgren-Miner's linear hypothesis. Numbers of cycles from Rainflow counting method for 10000 sec. data were extrapolated for 15 to 30 years life cycles. Typically, wind turbines or any other energy conversion devices are designed for 25-30 years against fatigue loads. Therefore, we designed the blade up to 30 years.

MATLAB was used to calculate fatigue damage by taking into account of Rainflow data and S-N data from ANSYS. The failure will consider when the accumulated damage exceeded 1.0. In figure 5.21, accumulated damage is plotted against number of years.
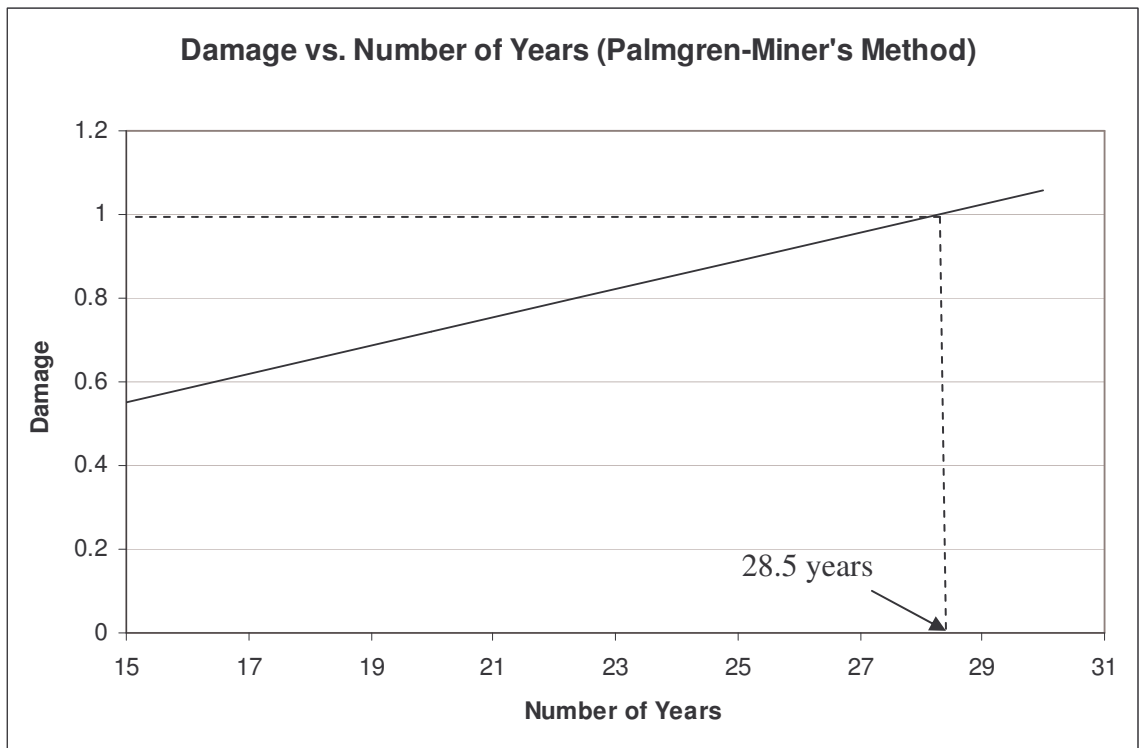
Figure 5.21: Accumulated Damage up to 30 years life

From this figure, a linear relationship between damage and operating years was found. This linearity could be explained from Palmgren-Miner's fatigue model as discussed in chapter 2. Damage varies linearly with operating life cycles for ideal case of fatigue analysis. It has been observed that accumulated damage will exceed 1.0 after 28.5 years of operating life. It means with the current loading conditions the modeled blade should be able to withstand until 28.5 years without any failure. The calculated damage involved applied stress cycles and fatigue behavior of the blade.

It should be mentioned here that there is a possibility of surface roughness due to corrosion and bio-fouling. Existence of any minute particle, or dislocation, or pre-crack was not considered in this analysis. These could cause stress concentration. All of these factors may have impact on fatigue behavior.

6.   SUMMARY

6.1   Summary

1. A sandwich composites construction with a single web is considered for OCT blade design. The core is made of polymeric foam while skin and web are made of carbon/epoxy and glass/epoxy composites, respectively.

2. OCT blade has been subjected to alternating loads originating from randomness of ocean current due to turbulence, and velocity shear.

3. The loads due to randomness of ocean current were found to be normally distributed with a mean of 40KPa and a standard deviation of 12KPa. Rainflow Counting Algorithm was used for extracting number of repetitions of load cycles with a specific mean and a loading ratio.

4. Variation in loads due to velocity shear was only 2% for a single revolution of the blade. This change of 2% load for a single revolution was associated with 6m change of depth.

5. A static analysis was first performed to determine the stress distributions along the entire length of the blade and identify the location of failure points. Separate failure criterion for composites and core materials was used. It was observed that a location near the root of the blade and at the joining of the web and skin was the most critical one.

6. A fatigue analysis was performed based on the stresses at the critical location. Four stress levels have been considered for fatigue analysis. The frequency of fatigue cycling was 1 Hz and the loading ratio was 0.1. Fatigue cycling at each stress level was continued until the Tsai-Wu failure criteria or factor of safety was reached. This defined the cycles to failure at that particular stress level and allowed the development of S-N diagram

7. S-N diagram revealed that the endurance limit of the blade was 48% of the ultimate shear strength of the core.

8. Accumulated damage was then calculated using Palmgren-Miner's linear rule. From damage analysis it was found that the blade will exceed damage factor 1.0 after 28.5 years - meaning that the blade will have a safe operational life of about 28.5 years under the given loading conditions.

6.2   Future Works

1. The loading spectrum has been extracted here based on approximated ocean current velocity distribution. For more accuracy, every second data is required. It should be possible by placing load cells attached with the blade and store the data for a several time periods.

2. In the current investigation, S-N diagram has been developed using finite element method. Some observations from this modeling were identical with previous works found in the literatures. But exact verification with composite blades under similar loading situation in an experimental set up was not performed. By making a prototype and using scaling laws one can attempt such verification.

3. General failure theories for isotropic and composite materials have been used to predict fatigue life. But for sandwich composites it is recommended that failure theories associated with face-sheet/core delamination, that is strain energy release rate (G_I) be also used.

4. Here fatigue loads due to velocity shear have been considered. Though the variation of loading due to velocity shear is very low (~ 2%) in our case, this will rise to 16% with turbine blade having 10m radius. Fatigue loads due to wake of ocean current has not been considered in the current study. This is also recommended to examine how loading will vary due to wake formation.

5. Temperature effect has not been considered although there is a temperature gradient along the depth of the ocean. Fatigue results may vary for large temperature variation. Degradation of material properties under sea water has not been considered either. Both of these factors may change fatigue life and need to be considered in future.

6. Surface of the blade is considered smooth in the investigation. But for underwater application there is a high possibility that blade surface will be contaminated by biofouling and affect the load distribution. Effect of biofouling on fatigue life may therefore be investigated in future.

7. During installation and scheduled maintenance events, turbine blades may experience very high amplitude loads for a short period of time. Such loading events also need to be considered in future.

8. No stress concentration has been considered. But to connect the blade with the hub by any bolted joint may cause stress concentration at the periphery of the hole. It is recommended to check for stress concentration near the hub.

APPENDIX

A.1   Blade Element Theory

Blade element theory relies on two key assumptions-

- There are no hydrodynamic interactions between different blade elements.

- The forces on the blade elements are solely determined by the lift and drag coefficients.

Each differential blade element of chord (c) and width (dr) located at a radius from the rotor axis is considered as a hydrofoil section]. BET is an iterative method which can be used to find an efficient hydrodynamic shape of a blade and the corresponding forces that act on it. Eight blade elements, or sections, of width 0.3 m were used for designing the proposed rotor blades. Figure A-1 contains an illustration of the loads that act on a local blade section.
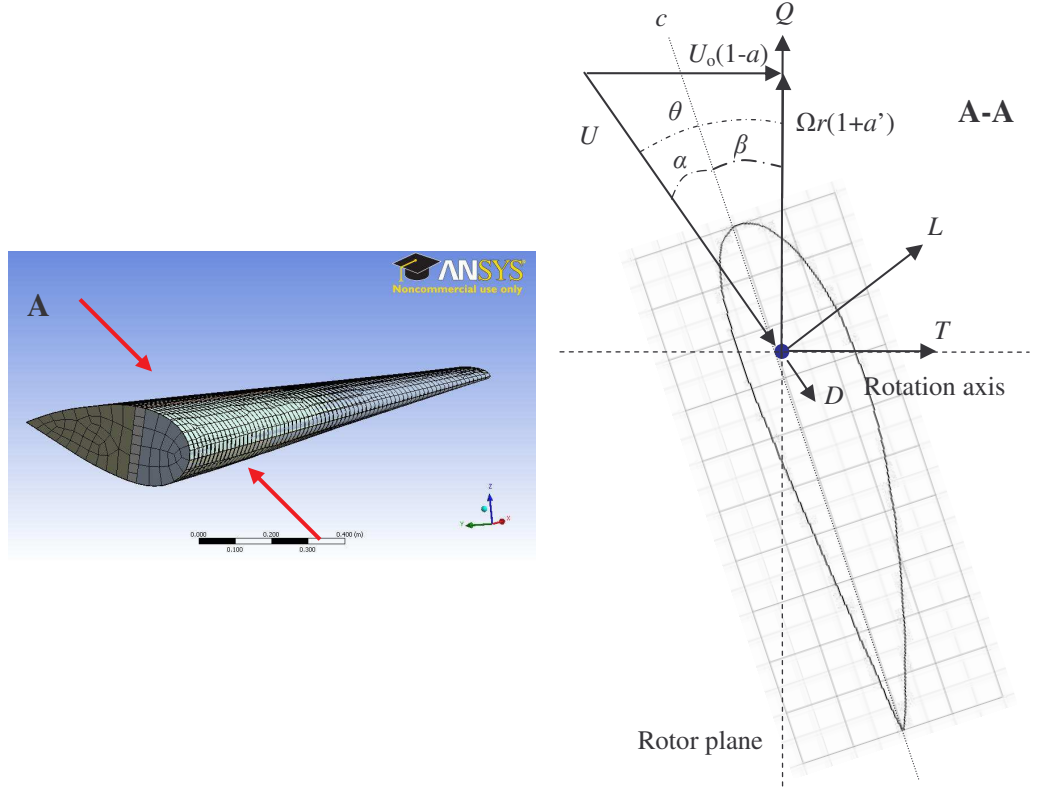
Figure A.1: Local blade forces and characteristics [11, 32, 41]

From Figure A.1 one can observe how a foil generates forces and see the directions in which they act. The pitch of the blade (β) is dependent upon the rpm, local radius (r), undisturbed free stream velocity (Uo), and design angle of attack (α). The inflow angle (θ) can be calculated using equation A-1.Variables 'a' and 'a'' are the axial and tangential induction factors, respectively. The axial induction factor accounts for induced velocity in the axial direction. The induced tangential velocity in the rotor wake is specified through the tangential induction factor [34].

$$\theta = tan^{-1}\left(\frac{U_0(1-a)}{\Omega r(1+a')}\right)$$

(A-1)

$$\alpha = \theta - \beta$$

(A-2)

Before loads can be determined, and design iterations started, some blade characteristics must be initialized. The high t/c values were needed for the required stiffness and strength. From the above equations and previously determined coefficients, the equations for calculating the local lift and drag loads are respectively:

$$dL = \frac{1}{2}\rho U^2 c C_L dr$$

(A-3)

$$dD = \frac{1}{2}\rho U^2 c C_D dr$$

(A-4)

Where ρ is the density of seawater, and C_L and C_D are the lift and drag coefficients, respectively.

The total loading was found by summing the loads calculated at the eight blade sections and multiplying that sum by the number of blades on the rotor disk.

In order to find the most efficient blade shape the following equations were also needed.

$$C_T = C_L \cos\theta + C_D \sin\theta$$

(A-5)

$$C_Q = C_L \sin\theta - C_D \cos\theta$$

(A-6)

$$\sigma(r) = \frac{c(r)N}{2\pi r}$$

(A-7)

$$a = \frac{1}{\dfrac{4\sin^2\theta}{C_T\sigma(r)} + 1}$$

(A-8)

$$a' = \frac{1}{\dfrac{4\sin\theta\cos\theta}{C_Q\sigma(r)} - 1}$$

(A-9)

where C_T and C_Q are the respective thrust and torque coefficients, and $\sigma(r)$ is the local blade solidity. Local blade solidity is defined as the fraction of the annular area in the hydrofoil section which is covered by the blades.

Steps involved in this iterative method are discussed below [11]-

1. Initialize a and a', set 'a' equal to 1/3 and 'a`' equal to 0.

2. Compute the flow angle (θ) using equation A-1.

3. Determine the local α using equation A-2.

4. Obtain $C_L(\alpha, Re)$ and $C_D(\alpha, Re)$ from DesignFOIL software.

5. Evaluate C_T and C_Q from equations A-5 and A-6.

6. Calculate a and a' using equations A-8 and A-9.

7. If da and/or da' are/is $\geq$ .01, go to step 1 and adjust factors.

8. If a is $\geq$ .4 adjust c and/or rpm and return to step 1, or finish.

9. Calculate the local loads using equations A-3 and A-4

The pressure load on the turbine blade, $P = \dfrac{dL}{cdr}$ (A-10)

So different element will be subjected on different pressure but for simplicity it has been assumed that all the elements will have under same pressure which is also average pressure on turbine blade.

A.2   Loads from Ocean Current

For fatigue analysis, each second velocity of ocean current data is required. But so far this data is not available. Rather than each second data annual and monthly data are available. Reeve and Driscoll's study on this revealed that the mean velocity of ocean current follows normal distribution. They have recorded data at every 30 minutes. For this limited data, we can approximate that the 10000 sec. data will also follow normal distributions. This approximation will not vary fatigue result significantly as we have used Palmgren-Miner's rule where loading sequences are not important. But for conservative design approach we have used the maximum mean of ocean current velocity and also maximum standard deviation. From their observed data it has been observed that maximum mean of the mean velocity is 1.86 m/s and maximum mean standard deviation is 0.275 m/s. Hence for 10000 sec. data we have assumed the maximum mean of 1.86 m/s and standard deviation of 0.275 m/s. Then 10000 samples have been extracted with a sampling frequency 1 Hz.

The distribution of the ocean current velocity is [42]–

$$f(u) = \frac{1}{\sqrt{2\pi}\sigma} \exp\left[\frac{-\left(u - \bar{u}\right)^2}{2\sigma^2}\right] \tag{A-11}$$

Here, σ = Standard Deviation

   $\bar{u}$ = Mean of ocean current velocity

The load and pressure on current is square function of ocean current velocity i.e. –

Load Pressure, $p = f\left(u^2\right)$ (A-12)

The mean and standard deviation of the load pressure has been determined from moment of random variable theory.

The mean of ocean current can be written as –

$$\bar{u} = \int uf(u)du \tag{A-13}$$

The standard deviation can be written as –

$$\sigma = \sqrt{\bar{u}^2 - (\bar{u})^2} = \sqrt{\int u^2 f(u)du - \left[\int uf(u)du\right]^2} \tag{A-14}$$

Replacing mean and standard deviation of ocean current velocity in equation (A-11) and replacing the function u with u^2 we will get the pressure distribution on turbine blade. MATLAB has been used for this complex computation and from MATLAB – mean pressure and standard deviation has been found 40KPa and 12KPa respectively.

BIBLIOGRAPHY

1. US Census Bureau. http://www.census.gov/popest/metro/CBSA-est2008-annual.html. Retrieved March 22, 2009.

2. Phillips, Pamela, and Gasparovic, Richard. "The Gulf Stream." The Gulf Stream. US Naval Academy, John Hopkins University. 1 July 2008. http://fermi.jhuapl.edu/student/phillips/

3. Stommel, H. "The Gulf Stream", University of California Press, Second Edition.

4. Lemanski, L. F., Coley, C.E., Goldberger, G. N., Dhanak, M. R., and Driscoll, F.R. "Center of Excellence in Ocean Energy Technology, Technical Proposal" 1 July 2008: 1-18. http://www.fau.edu/bot/files/COEOET_Doc.pdf

5. "Seaflow."MarineCurrent Turbines. 1 July 2008 http://www.marineturbines.com/6/background/14/seaflow/

6. "SeaGen." Sea Generation.1 July 2008 http://www.seageneration.co.uk/default.asp

7. "The RITE Project." Verdant Power. 1 July 2008 http://verdantpower.com/whatinitiative

8. Batten, W.M.J., Bahaj, A.S., Molland, A.F., Chaplin, J.R., "The prediction of the hydrodynamic performance of marine current turbines," Renewable Energy Volume 33, Issue 5, May 2008, Pages 1085-1096.

9. Bahaj, A.S., Molland, A.F., Chaplin, J.R., Batten, W.M.J., "Power and thrust measurements of marine current turbines under various hydrodynamic flow conditions in a cavitations tunnel and a towing tank," Renewable Energy Volume 32, Issue 3, March 2007, Pages 407-426.

10. Batten, W.M.J., Bahaj, A.S., Molland, A.F., Chaplin, J.R. "Hydrodynamics of marine current turbines," Renewable Energy, Volume 31, Issue 2, Marine Energy, February 2006, Pages 249-256, ISSN 0960-1481, DOI: 10.1016/j.renene.2005.08.020.

11. Asseff, N., Mahfuz, H., "Design and Finite Element Analysis of Ocean Current Turbine Blade", MS Thesis, Florida Atlantic University, August, 2009.

12. Sharma, N., Gibson, R., Ayorinde, E., "Fatigue of Foam and Honeycomb Core Composite Sandwich Structures: A Tutorial", Journal of Sandwich Structure and Materials, Volume 8:263, 2006.

13. Vinson, J.R., "The Behavior of Sandwich Structures of Isotropic and Composite Materials", Technomic Pub. Co., Lancaster, PA. 1999

14. Zenkert, D., "An Introduction to Sandwich Construction", Emas Publication, UK, 1997

15. Kanny, K. and Mahfuz, H., "Flexural Fatigue Characteristics of Sandwich Structures at Different Loading Frequencies", Composite Structures, 67(4): 403–410, 2005

16. Kulkarni, N., Mahfuz, H., Melanie, S. and Carlson, L.A., "Fatigue Failure Mechanism and Crack Growth in Foam Core Sandwich Composites under Flexural Loading", Journal of Reinforced Plastics & Composites, 23(1): 83–94, 2004.

17. Burman, M. and Zenkert, D.," Fatigue of Foam Core Sandwich Beams – 1: Undamaged Specimens", Int. J. Fatigue, 19(7): 551–561, 1997.

18. Burman, M. and Zenkert, D., "Fatigue of Foam Core Sandwich Beams – 2: Effect of Initial Damage", Int. J. Fatigue, 19(7): 563–578, 1997.

19. Sendeckyj, G.P.. Life Prediction for Resin-matrix Composite Materials, In: Reifsnider, K.L. (ed.), Fatigue of Composite Materials, 431–480, 1990

20. Dai, J. and Hahn, H.T., "Fatigue Analysis of Sandwich Beams using a Wear-out Model, Journal of Composite Materials, 38(7): 581–589, 2004.

21. Mahi, El A., Farooq, M.K., Sahraoui, S. and Bezazi, A., " Modeling the Flexural Behavior of Sandwich Composite Materials under Cyclic Fatigue", Materials & Design, 25(3): 199–208, 2004

22. Hashin, Z. and Rotem, A. . "A Cumulative Damage Theory of Fatigue Failure", Journal of Material Science Engineering, 34(2): 147–160, 1978

23. Wang, A.S.D., Chou, P.C. and Alper, J., "Effect of Proof Test on the Strength and Fatigue Life of a Unidirectional Composite", Fatigue of Fibrous Composite Materials ASTM STP, 723, 116–132, 1981.

24. Shenoi, R.A., Clark, S.D. and Allen, H.G." Fatigue Behaviour of Polymer Composite Sandwich Beams", Journal of Composite Materials, 29(18): 2423–2446, 1995

25. Shenoi, R.A., Wellicome, J.F., "Composite Materials in Maritime Structures: Fundamental Aspect", Cambridge University Press., UK, 1993

26. Suresh,.S. "Fatigue of Materials", Cambridge University Press,UK, 1998

27. Budynas, R. G., Nisbett, J. K., "Shigley's Mechanical Engineering Design", McGraw Hill, 2008.

28. Anderson, T.L. "Fracture Mechanics: Fundamentals and Applications", Second Edition, Boca Raton, FL Press, 1995.

29. Barsom, J.M., "Fatigue crack growth under variable amplitude loading in various bridge steels", Special Technical Publication, ASTM, pp 217-235, 1976.

30. Broek, D., "The Practical Use of Fracture Mechanics", Kluwer Academic Publishes, Page 186.

31. Manwell, J.F., McGowan, J.G., Rogers, A.L., "Wind Energy Explained: Theory, Design and Application", Wiley Publication, 2009.

32. Hansen, M., "Aerodynamics of Wind Turbines", Earthscan Press, London, UK, Second Edition, 2008.

33. Baek, S., Cho, S., Joo, W. "Fatigue Life Prediction Based on Rainflow Cycle Counting Method for the End Beam of a Freight Car Bogie", International Journal of Automotive Technology, Vol 9, pp. 95-101, 2008.

34. Daniel, Isaac, Ishai, Ori. Engineering Mechanics of Composite Materials. 2nd ed. New York: Oxford University Press, Inc., 1996.

35. Jones, R., "Mechanics of Composite Materials", Hemisphere Publication, USA.

36. Technical Manual: DIAB's Divinycell H, April 2010.

37. Kong, C., Bang, J. , Sugiyama, Y., "Structural Investigation of wind turbine blade considering various load cases and fatigue life", Energy, Volume 30, September 2005.

38. Raye, R., Driscoll, F. "Characterization study of the Florida current at 26.11 North Latitude, 79.50 West longitude for ocean current power generation", MS thesis, Florida Atlantic University, May 2002.

39. ANSYS, Inc. Release 11.0 "Element Reference", Part 1, Element Library 2007.

40. Kulkarni, N., Mahfuz, H., "Fatigue Crack Growth and Life Prediction of Foam Core Sandwich Composites under Flexural Loading", Composite Structures, Volume 59, March 2003, page 499-505.

41. Bertin,J.J., "Aerodynamic for Engineers", Prentice Hall, Fourth Edition, USA 2001.

42. Cooper, G., McGillem, C., "Probabilistic Methods of Signal and System Analysis", Oxford University Press, Third Edition, New York, USA,.